Evaluation of Stress Corrosion Cracking of High-Nitrogen Cr-Mn Stainless Steel

By

Lungile Ngubekhaya Mginqi

A dissertation submitted to the Faculty of Engineering in partial fulfilment of the degree of Master of Science in Engineering (Applied Science).

Department of Materials Engineering
University of Cape Town
December 1997

SYNOPSIS

The stress corrosion cracking susceptibility of an experimental high nitrogen Cr-Mn stainless steel, known as Cromanite™, and conventional AISI 304 stainless steel were investigated in order to compare their stress corrosion performance in solutions where AISI 304 stainless steel is known to be susceptible.

Slow strain rate tests (SSRT) were performed on solution treated specimens at 30°C in aerated aqueous sodium chloride (NaCl) solution containing hydrochloric acid (HCl) of varying concentration at open circuit potentials. Static tests in the form of bent-beam tests were performed on both solution treated and aged specimens in 3M NaCl solution containing 0.05 M HCl. Potentiodynamic scans and Tafel plots were used to assess corrosion behaviour and corrosion rate respectively, while the electrochemical potentiokinetic reactivation (EPR) method was used to quantify the degree of sensitisation for the materials.

The SSRT revealed poor corrosion behaviour of Cromanite™ in the presence of hydrochloric acid. Whilst AISI 304 could be examined for stress corrosion cracking at HCl concentrations up to 0.5 M HCl, Cromanite™ exhibited corrosion rates which were too fast to permit assessment of stress corrosion susceptibility at HCl concentrations of 0.15 M or above. SCC started in a salt solution containing 0.05M HCl for AISI 304 while Cromanite™ cracked in both salt solution (3 M NaCl) and in 0.05 M HCl + 3 M NaCl.

The bent-beam test performed on solution treated specimens revealed no evidence of cracking for both alloys after 100 days of exposure; however, Cromanite™ suffered substantial mass loss after this period. While aged Cromanite™ suffered intergranular cracking after only 25 days in the test solution, no cracking was observed for the aged AISI 304 after 75 days.

Potentiodynamic measurements demonstrated similar general corrosion properties in all environments tested. The EPR tests showed that AISI 304 stainless steel and Cromanite™, when tested in the solution treated condition performed equally well, but a comparatively poor performance of aged Cromanite™ was again demonstrated by this technique. It has been concluded that though the corrosion resistance of the alloys are similar, their stress corrosion properties are different because Cromanite™ sensitises easily on ageing.

ACKNOWLEDGEMENTS

I would like to express my most sincere appreciation to the following people who have assisted and guided me during the course of this project.

Dr. Rob Knutsen, my supervisor, who was a source of enthusiasm, encouragement and critical guidance throughout the project.

Messrs Glen Newins, Nick Dreze and Reggie Hendricks for their help and expertise in the workshop producing various specimens.

Mr. Dave Dean for his technical support and assistance with electronic equipment.

Mrs. M Topic for her assistance in the laboratory.

Messrs Bernard Greeves and James Petersen for their help in producing photographic prints.

Major thanks go to Columbus Stainless, Lucien Matthews, FRD and UCT Andrew Mellon Foundation for providing financial support in making this project possible.

Diteboho ho tswa botebong ba pelo ya ka ho motsoalle wa ka wa hlooho ya Kgomo Likonelo Makotoko. Modimo A be le wena.

Finally to all my colleagues and lecturers who made the experience in the department an enjoyable one.

Dedicated to makhulu Belina Ludidi *kanye nomama* Nomzamo Abigail Mginqi *for their unfailing support over the years.*

TABLE OF CONTENTS

LIST OF ABBREVIATIONS

AISI	American Iron and Steel Institute
ASTM	American Society for Testing of Materials
E_{corr}	Free corrosion potential
IGC	Intergranular Corrosion
HNSS	High nitrogen stainless steel
LVDT	Linear variable displacement transducer
MPa	Mega Pascal (=N/mm^2)
NaCl	Sodium Chloride
NaOH	Sodium Hydroxide
PESR	Pressurised electro slag remelting
PMMA	Polymethyl methacrylate
ROA	Reduction of area
SCC	Stress corrosion cracking
SEM	Scanning electron microscope
SCE	Saturated calomel reference electrode
SS	Stainless steels
SSRT	Slow strain rate testing
TM	Trade mark
UTS	Ultimate tensile strength
wt %	Weight percentage

Chapter 1 INTRODUCTION

1.1 Background to the research

Stress corrosion is the acceleration of the rate of corrosion damage by static stresses. Stress corrosion cracking (SCC) is the spontaneous cracking that results from combined effects of tensile stress, a susceptible microstructure and a corrosive environment. This synergistic effect causes macroscopically brittle failure of a component. In the absence of a corrosive environment, the material exhibits normal mechanical behaviour under the influence of stress. It has been established that prior to the development of a stress corrosion crack there is little deterioration of strength and ductility.

The most curious aspect of this phenomenon is that the component fails at loads below the design strength and the failure is preceded by a period of insidious slow crack growth. SCC can be reduced by changing the alloy microstructure or the surrounding environment or both, thus eliminating one of the components of the synergism mentioned earlier. The specificity of the material-environment couple is an important feature of environmentally assisted cracking. Certain materials will crack in an environment in which other materials perform satisfactorily.

At present the price of nickel has a considerable influence on the total cost of alloying elements in austenitic stainless steel. At the current nickel price level of US$8/kg, the cost of nickel alone accounts for 60% of the total raw material cost[1]. This state of affairs justifies an investigation to find a less expensive alternative alloy to nickel-bearing stainless steel. A suitable alternative would need to be one that is formable and ductile with a similar or superior combination of mechanical and corrosion properties.

The past developments in manufacturing techniques for the production of high nitrogen Cr–Mn steels and the good mechanical and corrosion properties of these alloys, combined with the high nickel price, are the factors that motivated this research. Central to the development of these steels is the very high strengths that can be attained (1000 MPa) without any reduction in fracture toughness, this despite the fact that the yield strength more than triples compared to nitrogen free austenitic stainless steel. These high strengths are as a result of the exceptionally high workhardening rate behaviour of these steels, an occurrence that has a positive spin-off to other mechanical properties, such as wear. Columbus Stainless is currently developing a high nitrogen Cr-Mn austenitic stainless steel which is known as Cromanite™. This study, which was commissioned by Columbus Stainless, Middelburg, South Africa, seeks to evaluate the stress corrosion cracking behaviour of Cromanite™ with a view of making it an alternative to nickel-bearing austenitic stainless steels.

1.2 Scope and limitations of the research

The aim of the study is to compare stress corrosion cracking susceptibility of a conventional nickel-bearing austenite stainless steel AISI 304 SS with an experimental nickel-free stainless steel, Cromanite™. This was carried out by exploring stress corrosion cracking in environments in which AISI 304 is known to be susceptible[2]. The conditions referred to range between 0.05 to 0.5 M HCl in a 3 M NaCl solution. This environment has consistently produced stress corrosion cracking in AISI 304 stainless steel at ambient temperature under open circuit potential conditions (OCP). These OCP conditions are experimentally desirable to eliminate the dependence of stress corrosion cracking on applied potential. The strain rate at which AISI 304 stainless steel is susceptible under these conditions could be reproduced with the equipment set-up used in the present study.

Stress corrosion cracking requires static tensile stress, corrosive environment and susceptible microstructure. The test methods adopted use both static (constant displacement test) and dynamic (slow strain rate test) stresses. The microstructure has been sensitised to achieve relative susceptibility between the experimental alloys. The degree of sensitisation (DOS) has been quantified with the use of EPR method. Corrosion testing in the same solution has been achieved by corrosion rate measurements using Tafel plots.

The scope of this research has been restricted to two compositions, i.e. AISI 304 and Cromanite™. As a result the influence of alloying elements on the stress corrosion behaviour of the alloy has not been assessed in this investigation.

The thesis is divided into six related parts. **Chapter 1**, Introduction, aims to outline the background, the scope and the limitations of the study. **Chapter 2**, Literature review, puts the research into context with the broader published scientific research. **Chapter 3**, Experimental techniques, describes material preparation and methods adopted in conducting the research. **Chapter 4**, Results, presents the findings of this work. **Chapter 5**, Discussion, puts the findings of this work into context with those of other workers. It also seeks to explain the phenomena observed, together with the apparent contradictions with the results of other workers. **Chapter 6**, Conclusions and recommendations, highlights conclusions which are considered to be important arising from the results of this work. It also suggests what could be done to improve the material under consideration.

Chapter 2 LITERATURE REVIEW

2.1 Introduction to stainless steels

Stainless steels (SS) have over the years become firmly established as materials for cooking utensils, fasteners, cutlery, flatware, decorative architectural hardware, and in vast numbers in equipment used in the chemical industry. SS are iron-based alloys that contain at least 12 wt % Cr which is the minimum amount required to prevent the formation of rust in unpolluted atmospheres[2-4].

The stainless property is achieved through the formation of a thin (5 nm), invisible and adherent chromium rich oxide film. This film forms and heals itself in the presence of an abundance of oxygen. SS are heavily alloyed : other elements added to improve particular characteristics include nickel, carbon, manganese, nitrogen, molybdenum, silicon, copper, cobalt, niobium, sulphur and selenium. Figure 2.1 provides a summary of some of the compositional and property linkages in the SS family.

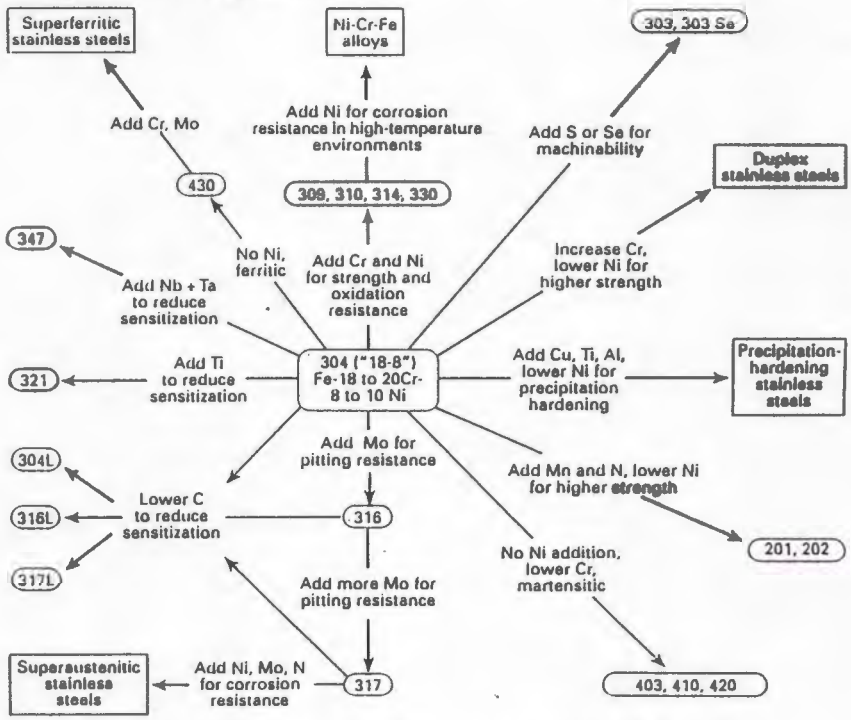

Figure 2.1: Compositional and property linkages in the SS family (after Sedricks[3]).

The development of the SS family has been slow due to several factors. Firstly, there has been difficulty in controlling alloying elements such as carbon, nitrogen and sulphur in prepared alloys due to poor refining techniques. Secondly, the cost of obtaining raw materials is a significant factor[4], particularly in the case of nickel which accounts for at least 60% of the cost of the raw material used in SS production[1]. These difficulties have led to the partial substitution of nickel by manganese and nitrogen such as is the case in AISI 200 series SS.

Several advances have been made in SS refining techniques, notably the adoption in the early 1970's of the Argon-Oxygen-Decarburisation (AOD) process[5]. This led to precise control of nitrogen and chromium during the SS production. Furthermore, it allowed the reduction of carbon and sulphur to exceptionally low levels when required. However, raw materials for SS remain expensive, and therefore a significant amount of effort is still required to find alternative elements to replace, in particular, nickel without compromising stainless properties.

2.1.1 Classification of stainless steels

SS can broadly be classified according to characteristic crystallographic structure into austenitic (fcc), ferritic (bcc), martensitic (bct), and duplex (bcc+fcc). A more recent development is the family of precipitation-hardenable alloys, based on the type of heat treatment used, rather than structure.

2.1.1.1 Austenitic stainless steels

The austenitic SS constitute the largest group of SS in terms of both the number of alloys and usage, accounting for approximately 70% of the family of SS[6]. They are non-magnetic, and possess excellent ductility, formability and toughness even at cryogenic temperatures. They can be substantially hardened by cold working.

Table 2.1 presents the mechanical properties of the commonly used austenitic SS. The example from the AISI 200 series is included to highlight the change in mechanical properties with the addition of nitrogen.

Alloy	Yield Strength (MPa)	Ultimate Strength (MPa)	Elongation (%)
AISI 304	205	518	45
AISI 316	205	515	45
AISI 201	260	655	45

Table 2.1: A few commonly used austenitic SS and their properties (after Novak[7]).

The mechanical properties of austenitic SS vary depending on the alloying element content. Some austenitic SS could become magnetic because of martensitic transformation when sufficiently cold-worked or heavily deformed. As a result they can exhibit a very high work hardening rate.

Another material property greatly affected by the character of the alloying element is the corrosion resistance. Figure 2.1 shows how the addition of molybdenum to AISI 316 (which becomes AISI 317) enhances corrosion resistance in chloride environments. Lower carbon grades, such as AISI 304L, have been established to prevent intergranular corrosion.

It is crucial to examine the role played by nitrogen in austenitic SS because the material of interest in this study is a high–nitrogen Cr-Mn SS where nickel is completely substituted by nitrogen and manganese.

2.2 *High–nitrogen Cr-Mn stainless steels*

An austenitic material is generally considered high-nitrogen if it contains nitrogen in excess of 0.4 wt %[8]. High nitrogen stainless steels typically contain no nickel; as a result other austenite stabilising elements are used. Nitrogen, being a strong austenite stabiliser is added for this function. Typical nitrogen contents range from 0.4 to 1.3 wt %.

The fundamental aspects of nitrogen's influence on the steel melt have long been known. The prediction of nitrogen solubility in liquid and solidified steels dates from before World War II. Figure 2.2 describes solubility limits for both carbon and nitrogen in steels. The maximum solubility of nitrogen in α- iron at the eutectoid temperature of 590°C is of the order of 1 atomic %, whereas at the same temperature of 590°C, it attains nearly 10 atomic % in γ-iron. This is larger than the maximum solubility of carbon in γ-iron at the eutectic temperature of 1153°C which is approximately 2.1 wt % or 6 to 7 atomic %. The difference is due to the fact that the size of a nitrogen atom is smaller than that of the carbon atom[9].

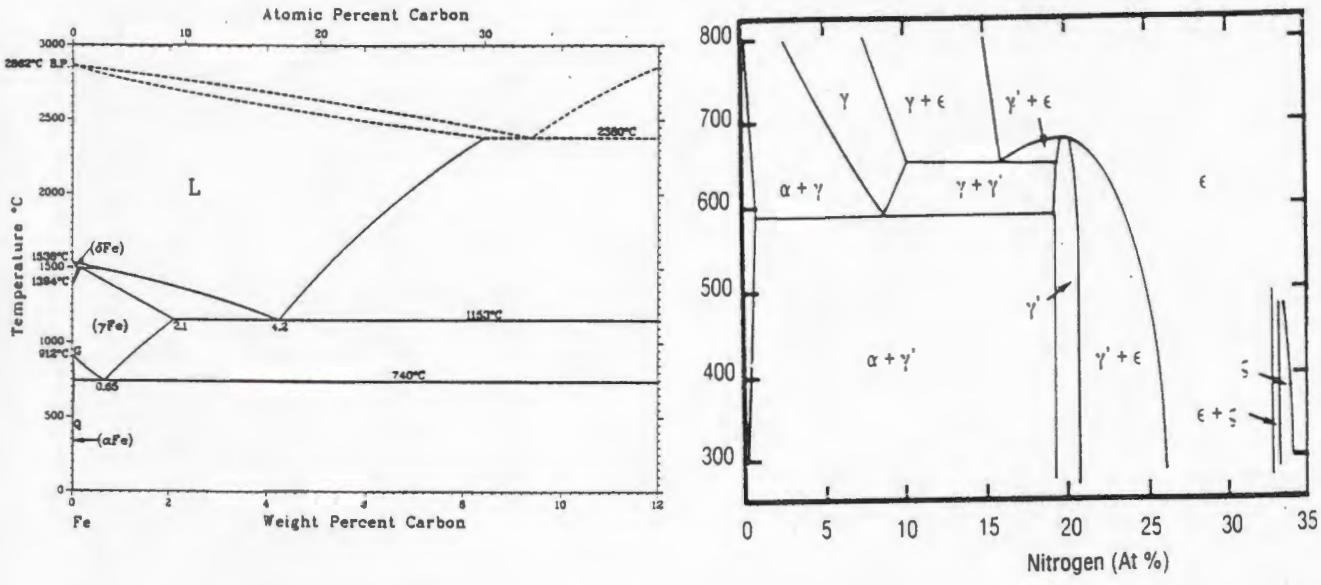

Figure 2.2: Solubility limits of carbon and nitrogen (after Lacombe[9]).

This work described above led to the realisation of the potency of nitrogen as an austenite forming element. Figure 2.3 shows the strength of nitrogen as an austenite forming element. It is important to note that nitrogen is twice as effective as nickel in reducing the enthalpy of austenite formation.

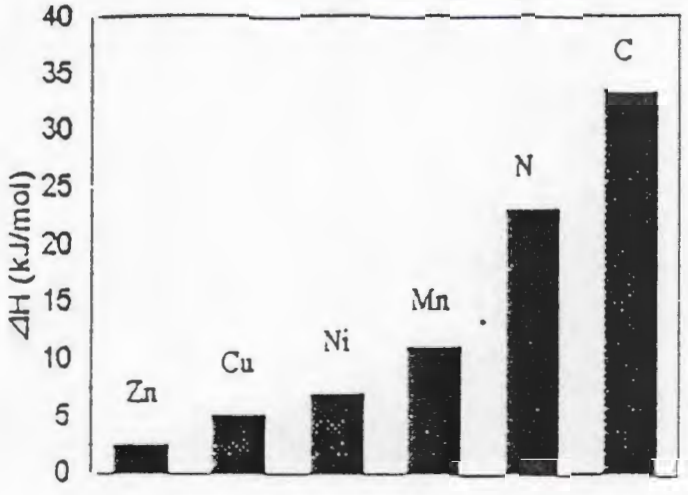

Figure 2.3: The effect of element addition on austenite phase stability (after Espy[10]).

Nickel shortages in Europe before World War II and in the US during the Korean War led to the use of manganese as a replacement for nickel in austenitic SS. Figure 2.3 shows manganese to be the next best stabiliser after nitrogen. The AISI 200 series was developed in the USA and introduced commercially in the 1950's[1].

Manganese thus gained superior status as an important constituent of SS, not for its alloying properties, but for economical reasons. It soon became evident that manganese alone could not be used to replace nickel. Nickel was thus reintroduced in reduced amounts and notably nitrogen was introduced.

Table 2.2 compares the composition of AISI 201 with commonly available austenitic SS.

Alloy AISI	Carbon [wt%]	Chromium [wt%]	Nickel [wt%]	Molybdenum [wt%]	Manganese [wt%]	Nitrogen [wt%]
304	0.08max	18 - 20	8 - 12	-	2 max	-
316	0.03max	16 - 18	10 - 14	2 - 3	2 max	-
201	0.15max	16 - 18	3.5 - 5.5	-	5.5 - 7.5	0.25

Table 2.2: Chemical composition of commonly available SS (after Pickering[11]).

The reason why nickel was not completely substituted with nitrogen at that time was that the production technology was not available then to enable SS to be alloyed with nitrogen above the solubility of nitrogen at atmospheric pressure[12]. In the 1960's much emphasis was placed on the study of solubility of nitrogen in iron alloys, particularly on the effect of other elements on the solubility of nitrogen.

Raweers and Kikuchi[13] derived equations to show the effect of Mn and Cr concentrations on the nitrogen solubility. Figure 2.4 shows the theoretically derived solubility of nitrogen as a function of Cr and Mn concentrations in samples melted at 1650°C and 200 MPa of nitrogen pressure.

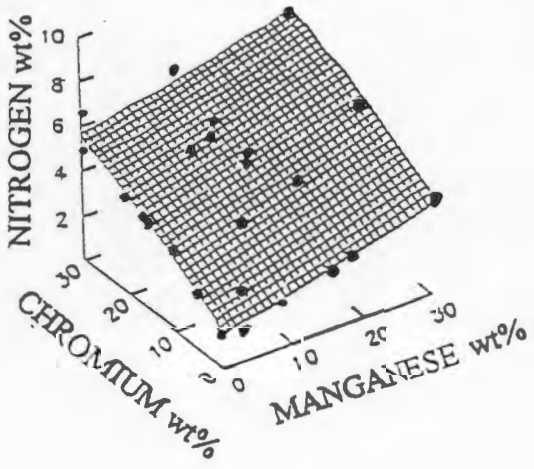

Figure 2.4: The variation of nitrogen solubility with addition of Cr and Mn (after Rawers and Kikuchi[13]).

Raweers and Kikuchi[13] concluded that manganese improves the solubility of nitrogen in the SS melt rather than stabilising the austenite phase. Other elements besides Mn, can be used to increase the solubility of nitrogen; the effect of these elements on nitrogen solubility is given in figure 2.5.

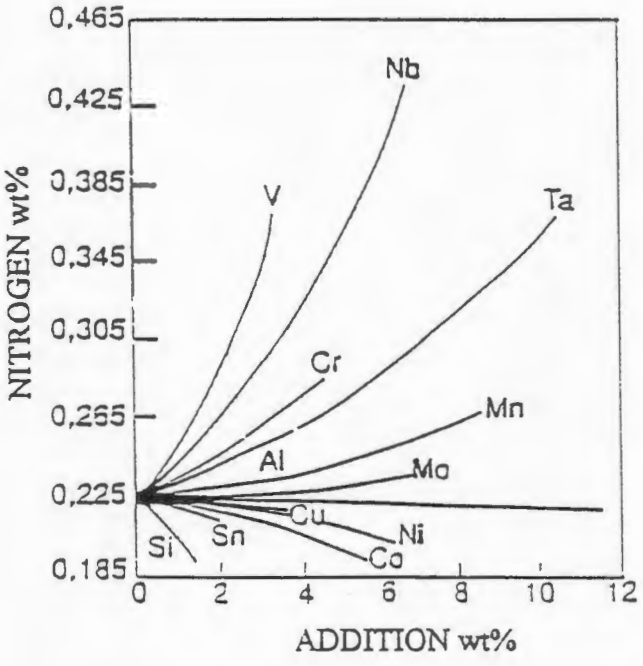

Figure 2.5: The effect of alloying elements on the solubility of nitrogen in a Fe18Cr8Ni melt at 1600°C and 1 atm. N_2 (after Irvine[14]).

Figure 2.5 shows that one way to obtain high nitrogen concentrations in a SS melt at 1 atm. N_2 would involve the use of alloying elements; the most effective would be vanadium, niobium, tantalum, etc. Unfortunately most elements that provide a strong positive action on nitrogen solubility also show strong nitride precipitation at low nitrogen concentrations. If this happens the element disappears into the slag[14]. It is sufficient to say that few elements fulfil the desired compromise of both marked positive action on solubility and suppressed nitride formation; Cr, Mn and Mo being the most important examples.

Once the knowledge of solubility of nitrogen in austenite was available, the effort was directed mainly at the manufacturing process technology. Manufacturing technology is a combination of two philosophies[12]. One aspect is the scientific validity, where thermodynamics and kinetics are decisive, but there is also the economic aspect, which determines whether or not even the most technically elegant manufacturing procedure will be economically realisable.

Several production techniques have been developed that allow production of high–nitrogen Cr–Mn SS in commercially viable quantities. The state of the art in the industrial manufacture of new high–nitrogen Cr-Mn alloys has been reviewed by several authors[12-15]. The most commonly used method is pressurised electroslag remelting (PESR)[15], in which the alloying is performed at high nitrogen partial pressure and nitrogen is either bubbled through the melt or added as nitrogen–rich ferrochrome powder.

The recent interest in high–nitrogen Cr-Mn SS, brought about by the attractive mechanical and comparable corrosion properties of these alloys, resulted in several extensive studies in their properties. Uggowitzer et al.[16] reported a five–fold improvement in the strength of a material in alloying with nitrogen from 0 wt % to 0.5 wt % in Cr–Ni and Cr-Mn steels. The strength is also increased by cold deformation and the effect is well documented[17]. Nitrogen strengthens the material mainly through a solid solution strengthening mechanism.

Figure 2.6 below illustrates the relative strengthening effects of different alloying elements. The figure shows that interstitial elements carbon and nitrogen have the greatest solid solution strengthening effect.

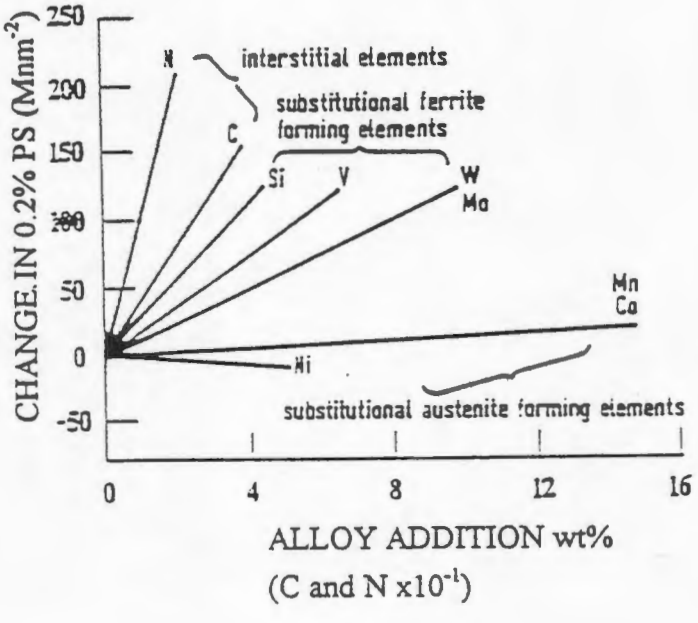

Figure 2.6: The solid solution strengthening effects of alloying elements in an austenitic SS (after Speidel[17]).

2.3 Corrosion

2.3.1 General corrosion

Corrosion is a gradual removal or alteration of a material by a chemical or electrochemical oxidising process. Corrosion in metals, whether in the atmosphere, underwater or underground, is caused by a flow of electric charge from one metal to another metal, or from one part of the surface of one piece of metal to another part of the same metal where conditions permit the flow of electricity. The presence of an electrolyte is a key condition for the process of corrosion to occur.

In a simple anodic dissolution process in water, metal enters solution as cations or hydrated ions following the equation of the type:

$$M \rightarrow M^{n+}(aq) + ne^- \qquad (2.1)$$

The anodic reaction produces electrons which must be consumed by an appropriate cathodic reaction. Under aerated conditions, this may be the Oxygen Reduction Reaction (ORR), represented by:

$$2H_2O + O_2 + 4e^- \rightarrow 4OH^- \qquad (2.2)$$

or, in de-oxygenated acidic environments, the Hydrogen Evolution Reaction (HER), represented by:

$$2H^+ + 2e^- \rightarrow H_2 \qquad (2.3)$$

It is important to note that since the electrochemical circuit must be completed for corrosion to take place, the removal of electrons may be controlled by the

cathodic reactions under certain conditions. These conditions could be a limited supply of oxygen, or difficulty of forming and removal of hydrogen gas bubbles.

The most frequent types of corrosion, some of which can occur simultaneously and those which require tensile stresses are illustrated in the figure 2.7.

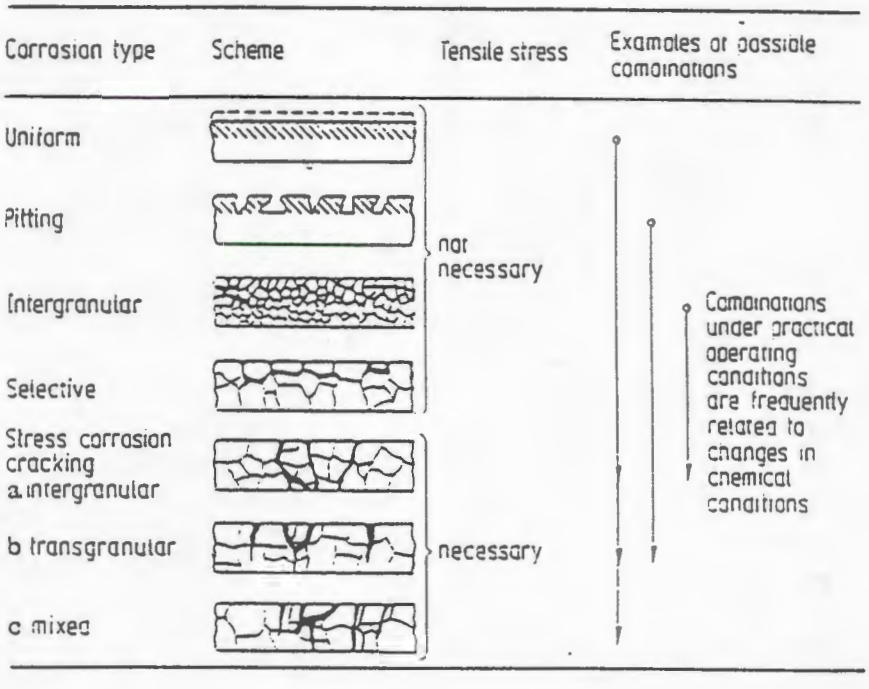

Figure 2.7: Schematic representation of common types of corrosion (after Fontana[18]).

2.3.2 Stress corrosion cracking

Stress corrosion cracking (SCC) is a progressive fracture mechanism in metals that is caused by the simultaneous interaction of a corrodent and a sustained tensile stress. Structural failure due to SCC is often sudden and unpredictable, occurring after as little as a few hours of exposure, or after months or even years of satisfactory service. The tensile stresses necessary for SCC are static and they may be either applied or residual, or both. Since SCC requires tensile stresses, a specific environment and a susceptible alloy, removal of any one of

these agents will terminate, prevent or delay the cracking process. Virtually all alloy systems are susceptible to SCC by a specific corrodent under a specific set of conditions.

Table 2.3 lists common engineering materials and environments in which they are susceptible to SCC.

Material		**Susceptible Environment**
Copper alloys		Ammoniacal
Aluminium alloys		Chlorides
Steels	mild	Hydroxides, nitrates, ammoniacal
	AISI 300 series	Chlorides, sulphates
	martensitic	Water, chlorides

Table 2.3: Susceptible material - environment couples (after Meletis[19]).

Stress corrosion cracking as a failure mode achieved engineering significance through the "season cracking" of brass cartridge cases in India and the "caustic embrittlement" of riveted steel boilers in early steam locomotives[20]. This failure is a brittle fracture of a material that would normally exhibit ductile behaviour under the influence of stress. The fracture surfaces have little or no evidence of accompanying plastic flow. Cracks propagate on a plane perpendicular to the

principal tensile stress in an inter- or transgranular manner depending on the particular alloy and environment.

Newman and Procter[21] defined SCC as a combination of physical and chemical processes that accomplishes the separation of bonds at the crack tip, thereby advancing the crack. The shear process leads to a local failure of the passive layer (section 2.3.3) at the end of the slip step.

The electrolyte attacks the free metal surface at the slip step, causing rapid anodic dissolution and removal of the metal (see figure 2.8). This formation is completed at such a speed that only the crack tip remains active, or free of a passive layer, thus the anodic dissolution is concentrated on this crack tip[22].

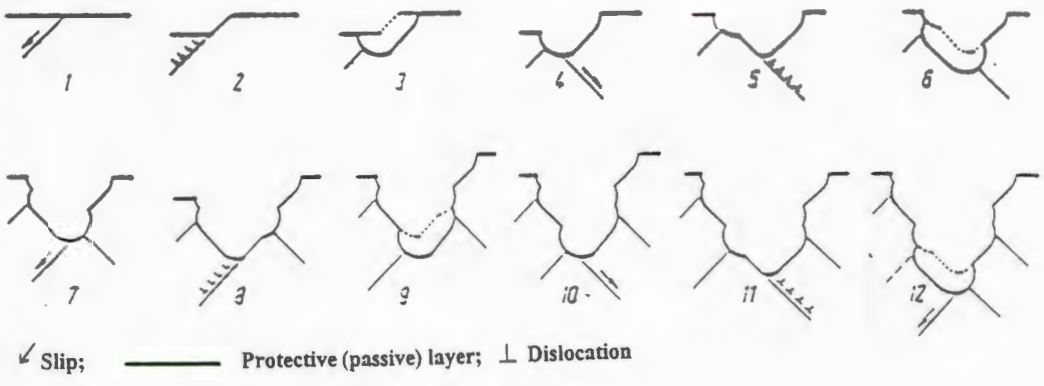

Figure 2.8: The model of crack growth by stress corrosion cracking (after Sriyatsan[22]).

It is an alternating process of destruction of protective film by slip processes, anodic metal dissolution and new formation of the layer. A layer of formation which forms too fast, would lead to immediate passivation of the crack tips and

therefore to the termination of the crack growth. However, a layer which forms too slowly would undergo general corrosion[23].

2.3.3 Passivation

The formation of an adherent and impervious surface film in effect stifles anodic dissolution (i.e. equation 2.1). The protection afforded by the surface film is dependent upon the chemical composition and the degree of mechanical perturbation which may rupture the film to expose bare metal surface. The chemical stability is affected by the acidity level and applied potential.

Sedricks[24] models the film as a hydrated oxide layer with gel-like structure. The model suggests that metal ions produced by anodic dissolution pass into solution through an underdeveloped area in the film. They become linked to water molecules and join the film with a simultaneous release of hydrogen. Other models suggest that a film is composed of a crystalline oxide. In all these models, the driving force for growth and stability is the existence of a potential between metal and solution, thus creating a strong electric field at the metal-solution interface.

The growth of a passive film occurs in a step manner, so that the active area from which the metal dissolves decreases with time. In an environment with excess of oxygen, the time to achieve passivation would be very brief[25]. This passive layer is only able to form over a specific potential range, as illustrated in figure 2.9, and it has been found that the critical potential ranges for stress corrosion cracking of passivating materials lie in the regions of active to passive transition[26].

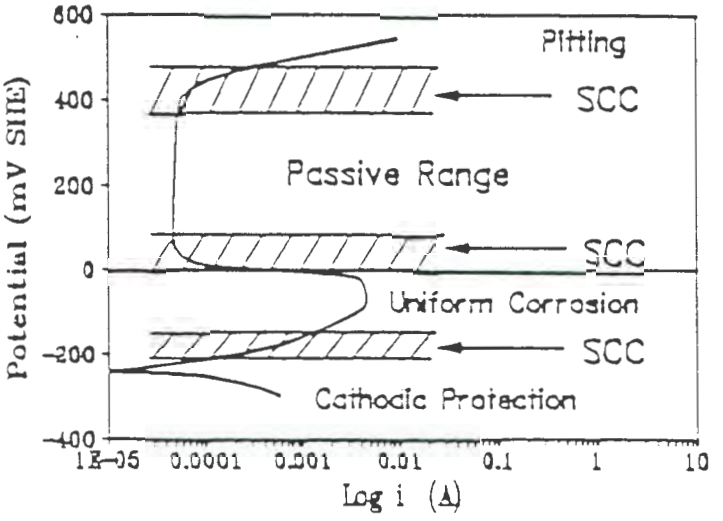

Figure 2.9: Stress corrosion cracking occurs near the active to passive transition potential in passivating steels. A schematic diagram for AISI 304 SS in 1N sulphuric acid solution (after Briant[26]).

The repassivation rate is an important consideration in stress corrosion cracking. It is in direct competition with rate of crack tip growth, which exposes fresh metal surface at the crack tip[27-30]. Slow repassivation rates result in crack blunting and possible crack arrest, due to excessive metal dissolution at both the crack tip and adjacent walls. Higher repassivation rates minimise the amount of crack penetration per oxide rupture event.

Rimbert[23] noted that maximum susceptibility occurs when repassivation rate is balanced by crack tip strain rate. This means that alloys susceptible to stress corrosion cracking in a particular solution have to repassivate at a particular rate, otherwise they undergo general corrosion due to lower repassivation rates or show stress corrosion cracking resistance due to higher repassivation rates. The repassivation rate is dependent upon the electric potential, local environment and, more importantly, the alloy composition.

2.3.3.1 *Alloying influences on passivation*

The repassivation behaviour in steels is heavily influenced by the alloying elements. However, alloying elements in turn can determine the microstructure, which has a direct consequence on the corrosion characteristics of the metal. A logical way to handle such a complex disposition of metallurgical variables is to examine how each variable affects the passivity parameters such as the passive potential range and pitting potential, to identify the variables which enhance passivity, and ideally, to identify a model that incorporates the individual effects.

2.3.3.1a Chromium

Chromium is the one element responsible for forming a passive film. No other element can by itself create the properties of SS as chromium does; however, other elements can influence the effectiveness of chromium in forming or maintaining the film. Several attempts to reduce chromium content to below 11 wt % and still maintain stainless properties have been unsuccessful[31]. Figure 2.10 shows the effect of reducing chromium on the anodic polarisation behaviour of the metal.

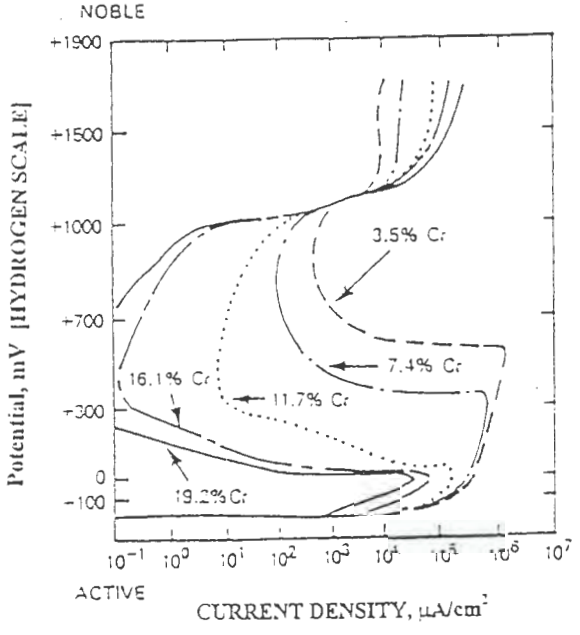

Figure 2.10: The effect of chromium content of FeNiCr alloys on their anodic polarisation behaviour in 2N sulphuric acid solution at 90°C (after Chen and Stephens[31]).

Figure 2.10 shows that alloying with chromium expands the passive potential region and reduces critical current density of the alloy. Increasing Cr content from 18 wt %, (which is typical of most of the AISI 300 series austenitic SS) to 29 wt %, such as in superferritic, greatly enhances the stability of the passive film. However, high Cr may adversely affect mechanical properties, fabrication, weldability and high temperature properties. Therefore, it is prudent to improve corrosion properties by altering other elements without increasing Cr content.

2.3.3.1b Nickel

Nickel is mainly used to stabilise the austenitic structure, which greatly enhances mechanical properties and fabrication characteristics. In reducing environments, nickel is effective in promoting repassivation, and therefore is particularly useful in resisting corrosion in mineral acids[11]. The addition of nickel affects the ability of the metal to passivate, both in the presence and in the absence of nitrogen. Stanko and Wellbeloved[32] found that corrosion rate dropped sharply with the reduction of nickel to less than 2 wt % but slowly approached that of Cr-Ni SS at 4 wt % Ni. They concluded that the minimum amount of nickel of 2 wt % is desirable in high–nitrogen Cr-Mn SS. Figure 2.11 shows the results of that study.

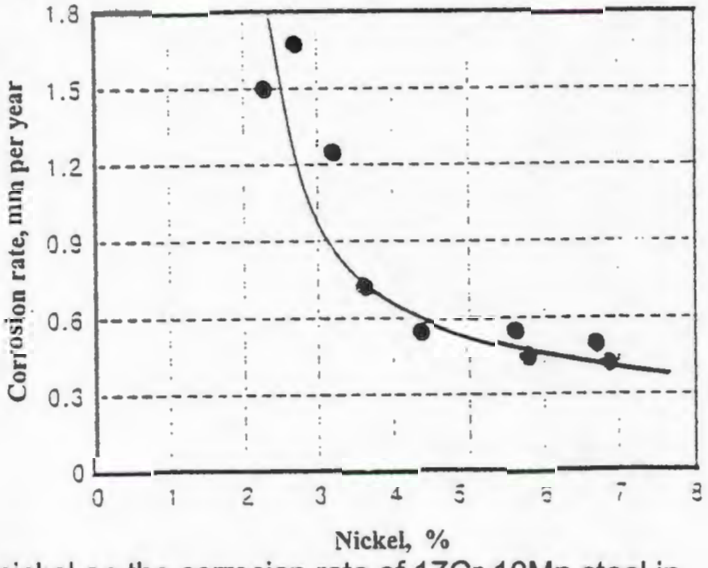

Figure 2.11: The effect of nickel on the corrosion rate of 17Cr-10Mn steel in boiling 65% nitric acid (after Stanko and Wellbeloved[32]).

In the absence of nickel Fourie[33] suggested the addition of 1 wt % copper to high nitrogen Cr-Mn stainless steel to improve the ability of the alloy to passivate.

2.3.3.1c Manganese

Manganese in austenitic SS is unique. It is responsible for the increase in nitrogen solubility without any danger of stabilising a nitride phase[34]. Manganese increases the nitrogen solubility much more in the solid state than in the liquid state[35] of SS, as shown in figure 2.12.

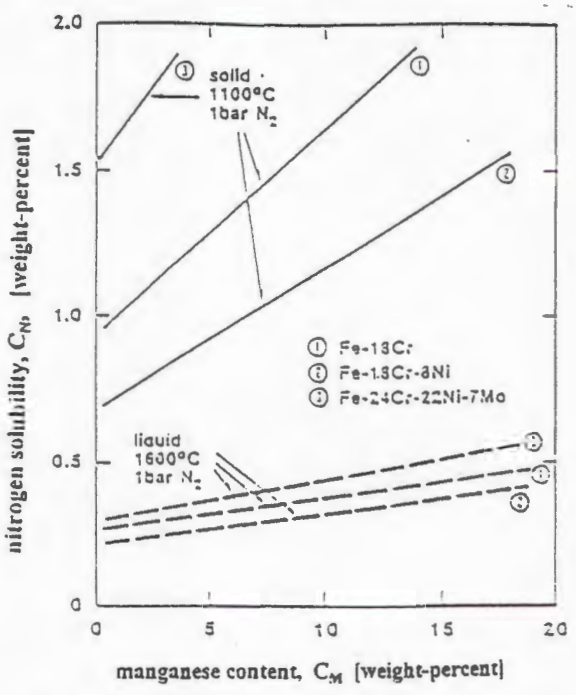

Figure 2.12: Effect of Mn on the nitrogen solubility in SS (after Speidel and Uggowitzer[35]).

Figure 2.12 also shows the dependence of nitrogen solubility on other alloying elements present, nickel being detrimental, chromium and molybdenum being beneficial to N_2 solubility. Manganese also performs functions similar to those attributed to nickel, such as stabilising the austenite phase. However, total replacement of nickel by manganese is not practical; this factor was demonstrated by the poor corrosion performance of the initial nickel-free AISI 200 series. It has also been found that manganese SS with equal chromium

content to nickel-bearing SS do not exhibit the same passivation, the reason being that Mn is more electrochemically active and undergoes selective dissolution faster than other elements. This is generally confirmed by polarisation curves which show that at any given potential the current density of Mn SS is higher than that of AISI 304 SS[39].

SCC tests done on Mn SS show that these steels are more susceptible to cracking than AISI 304 SS[39]. These results showed SCC to be dependent on the amount of nickel present in the SS. Manganese interaction with sulphur is known to be detrimental in SS as it results in the formation of manganese sulphides. The morphology and composition of these sulphides can have substantial effects on corrosion resistance, especially pitting resistance[3].

2.3.3.1d Molybdenum

It has long been known that, for a given Cr content in a SS, the addition of molybdenum has a strong beneficial influence on passivity. Molybdenum moves the pitting potential in the noble direction, thereby extending the passive region. In Cr-Mn steels addition of molybdenum and nitrogen have been found to reduce the corrosion rate[36]. The mechanism by which molybdenum exerts its influence is not yet well understood. Molybdenum appears to hinder both the breakdown of passivity by pitting and the growth kinetics of pitting[37].

2.3.3.1e Molybdenum plus nitrogen

Nitrogen has been shown to enhance the effects of molybdenum in improving localised corrosion resistance and passivation characteristics through an apparent synergism that is not fully understood[38]. It has been suggested that during active dissolution and passivation, nickel, molybdenum and nitrogen are enriched strongly in the alloy surface below the oxide passive film of austenitic SS.

Since nickel does not participate directly in the formation of passive films of austenitic SS, most models of passivity try to explain the corrosion behaviour in terms of chromium, molybdenum and nitrogen. Devasenapathi et al.[39] recently reported that metallic nickel underneath the passive film was enriched during anodic polarisation. This suggests that nickel contributes to passivation and improved pitting resistance through reduction of the anodic dissolution rate following strong intermetallic bonding with chromium and molybdenum in the presence of nitrogen[40]. However, further work is needed to develop fully this model.

2.3.3.1f Nitrogen

It has long been known that nitrogen additions are beneficial to the development of passivity in austenitic SS in sulphuric acid solutions[3]. Figure 2.13 shows that nitrogen moves the pitting potential in the noble direction, thereby extending the passive potential range.

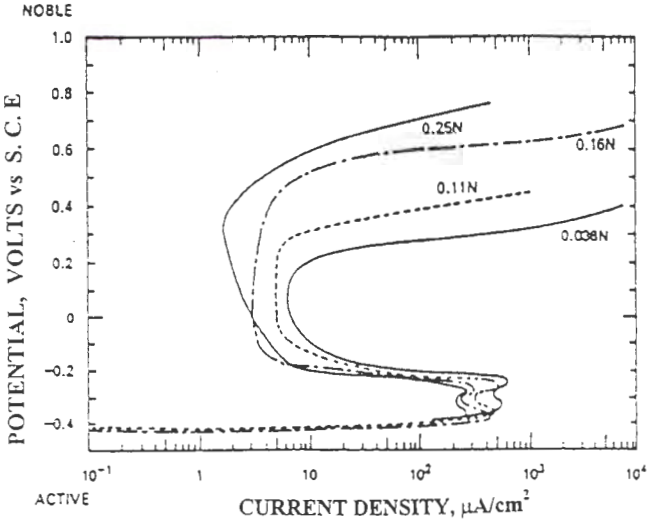

Figure 2.13: Anodic polarisation curves for 18%Cr-8%Ni SS containing various amounts of nitrogen in 1N sulphuric acid + 0.5 M NaCl solution at ambient temperature (after Eckenrod and Kovach[41]).

It remains unclear if nitrogen alone in the absence of molybdenum is capable of improving the corrosion properties in SS[38]. In order to clarify this, Beneke and Sandenbergh[42] investigated the role of nitrogen in dissolution and passivation of AISI 304 austenitic SS. They concluded that nitrogen addition up to 0.15 wt % does appear to improve general corrosion resistance of the alloy and further additions in excess of this amount decreased the corrosion resistance. However contradictory results[44] have recently been reported where nitrogen at 0.58 wt % was found to improve the repassivation behaviour of both Cr-Mn and Cr-Ni steels in the presence of chloride anions using a scratch technique. The authors invoked three different models to explain this increase in corrosion resistance of these steels. They are :

1. Consumption of acid in pit nuclei by nitrogen dissolution and ammonium ion formation;

2. Enrichment of nitrogen on the passivated surfaces at the film / metal interface, which may lead to desorption of the aggressive anions (Cl^-) upon breakthrough of the passive layer; and

3. Enrichment of nitrogen on the active surfaces, which is assumed to cause kink blockage preventing the attainment of high current densities necessary for the pit initiation.

Since scratching exposed bare metal surface to the environment the authors concluded that the enriched nitrogen at the interface contributed to the improved corrosion resistance[44].

Nitrogen has normally been regarded in much the same light as carbon because the two lie alongside one another in the Periodic Table of the

Elements and impart similar properties to steels. The solubility of both elements was discussed in section 2.2. It is well documented that the carbon content of steel influences the stress corrosion properties of the steel. The increase in the carbon content of an alloy results in the increase of stress corrosion crack velocities[43-45]. This fact was illustrated by Pedrazzoli and Speidel[46], as shown in figure 2.14.

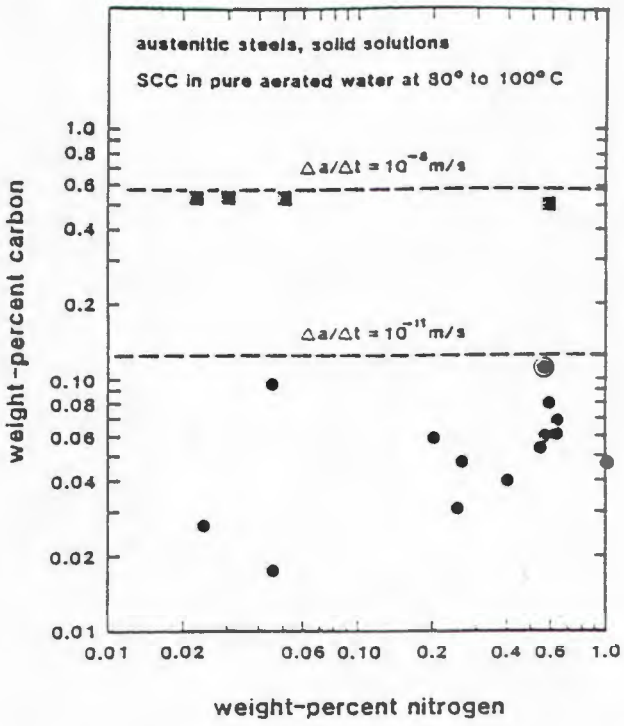

Figure 2.14: The effect of nitrogen and carbon on the growth rates of stress corrosion cracks of austenitic SS (after Pedrazzoli and Speidel[46]).

The unanswered question appears to be whether it is the absence of carbon or, eventually, the presence of nitrogen which imparts the positive results to stress corrosion properties of austenitic SS. Figure 2.14 also shows that SCC growth velocities are independent of nitrogen content. Thus the indication to date (in the absence of a convincing mechanism) is that nitrogen is the only element in austenitic SS that allows the production of carbon-free austenitic steels with sufficient strength.

2.3.3.1g Other alloying elements

Vanadium, silicon and tungsten are also known to extend the pitting potential in the noble direction[47], thereby extending the passive region. Figure 2.15 summarises the effect of various alloying elements on anodic polarisation curves in 0.1 M HCl. High silicon SS that contain up to 4 wt % of Si have found great use in highly oxidising environments.

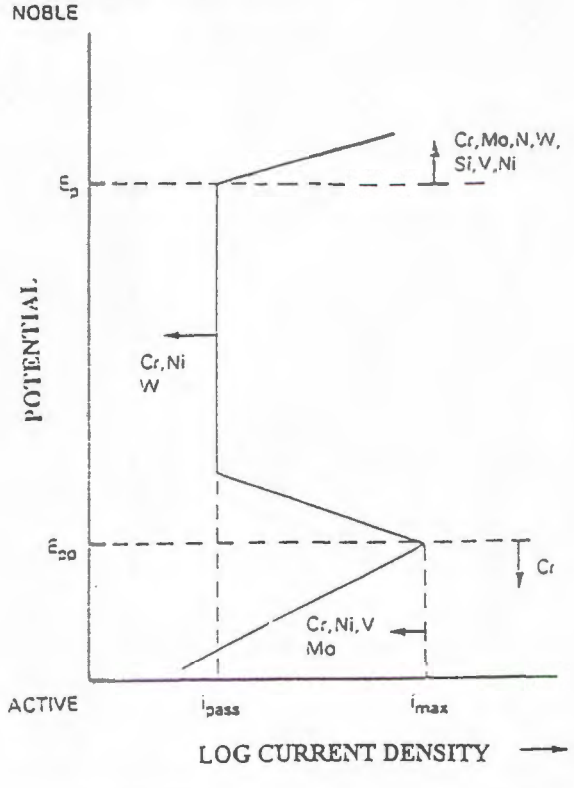

Figure 2.15: A schematic summary of the effect of alloying elements in stainless steels on the anodic polarisation (after Sedricks[24]).

2.3.3.1h Metallurgical factors

SS achieve their high corrosion resistance when more than 12 to 13 wt % of Cr, depending on the environment, is present in the matrix of the steel. It is now well established that when these steels are slowly cooled from a solution annealing temperature of 1050°C, or are heated in the temperature range of 400°C to 850°C, precipitation of carbides is promoted[46,48-50]. This phenomenon is known as sensitisation. The presence of precipitates at grain boundaries renders the alloy susceptible to severe intergranular corrosion (IGC).

The most widely accepted explanation of this IGC susceptibility is based on the chromium depletion model. This model postulates that the growth of Cr-rich precipitates at grain boundaries in sensitised SS leads to a Cr-depletion region (below 12 wt %) in the matrix at and immediately adjacent to the grain boundary. Parkins[51] has reviewed other models that purport to explain the IGC susceptibility: these are described below.

(1). The noble carbide theory postulates that the IGC results from a galvanic coupling of the matrix metal with the noble carbides, causing an electrochemical reaction between the carbides and the matrix along grain boundaries[47];

(2). The solute segregation model postulates that the presence of a continuous second phase along the grain boundaries causes them to be preferentially attacked[50]; and

(3). The strain theory postulates that since the lattice adjacent to the Cr carbides is distorted and hence has a higher strain energy than the matrix, these regions are prone to intergranular attack[49].

Most of the Cr-rich precipitates have been identified as Cr carbide of the $[Fe,Cr]_{23}C_6$ form[52]. Decreasing carbon to the lowest possible level will reduce the susceptibility to IGC. However, this reduction of carbon will degrade the mechanical properties such as the yield and tensile strengths.

It has been established that nitrogen additions can retain or improve mechanical properties of austenitic SS. The object of replacing carbon with nitrogen would be expected to benefit the metal in two ways :

(1) Since the nitride precipitation is of the form of Cr_2N, on a mole per solute basis, less Cr is precipitated by N than C, assuming stoichiometric composition[50].
(2) When nitrogen is in the solid solution it has the effects of retarding the kinetics of formation of second phases such as chi and sigma[53].

Figure 2.16 shows the effect of nitrogen in delaying the onset of $M_{23}C_6$ precipitates.

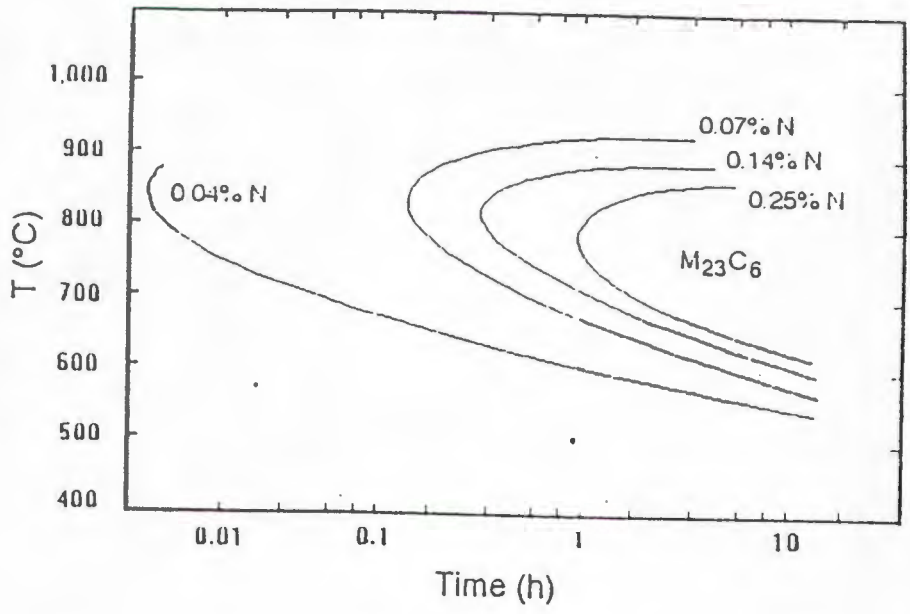

Figure 2.16: The effects of nitrogen on the precipitation kinetics of $M_{23}C_6$ (after Mozhi[54]).

For the type AISI 304 SS, Mozhi et al.[54] found that nitrogen content up to 0.16 wt % retarded sensitisation kinetics of formation of $M_{23}C_6$ but that nitrogen had no significant effect at 0.25 wt %. The authors concluded that the precipitation of Cr nitrides became significant at nitrogen content higher than 0.16 wt % and that nitrogen additions in excess of this amount contributed to intergranular corrosion attack.

Mozhi et al.[53] in a separate investigation, examined the effect of nitrogen on stress corrosion cracking of AISI 304 SS in chloride and sulphate solutions. They found that nitrogen additions up to 0.16 wt % increased the SCC resistance, while a nitrogen addition of 0.24 wt % decreased it.

Since high–nitrogen SS, (i.e., N content > 0.4 wt %) exceed the optimal amounts of 0.16 wt %, they should suffer from intergranular corrosion resulting from formation of these Cr precipitates. This severely reduces the fracture toughness though these steels possess the highest combination of strength and fracture toughness for all materials[46].

2.4 Mechanisms of stress corrosion cracking

Since the 1960's three generally accepted mechanisms have emerged though others exist[55,62]. These mechanisms are pre-existing active path, strain-assisted active path and adsorption-related phenomena.

The formation of an occluded cell in which the environment is concentrated often precedes cracking in all SCC mechanisms. This occluded cell can be a result of bad design, surface roughness and crevice situations so that the corrosive attack is progressive even before the plant is commissioned. The duration of the crack initiation process commonly accounts for most time to

failure. Initiation is followed by slow insidious crack propagation which can occur by any of the mechanisms discussed below.

2.4.1 Pre - existing active path mechanism

Grain boundaries have an energy field associated with the atomic mismatch which make them favourable sites for impurity segregation and solute precipitation. Grain boundary dislocation pile–up further increases this activity. This strain energy encourages dissolution reactions, providing the driving force for stress–assisted intergranular corrosion cracking. In SS the formation of chromium carbides at grain boundaries or at deformation sites within the grains can lead to stress corrosion cracking by this mechanism[56]. Figure 2.17 shows a schematic diagram of crack propagation along a sensitised grain boundary. The sensitised grain boundary is locally depleted of chromium due to precipitation of carbides or nitrides. This decreases the repassivation rates in the vicinity of the grain boundaries. Intergranular corrosion occurs if the grain is chemically active with respect to the grain interior[57].

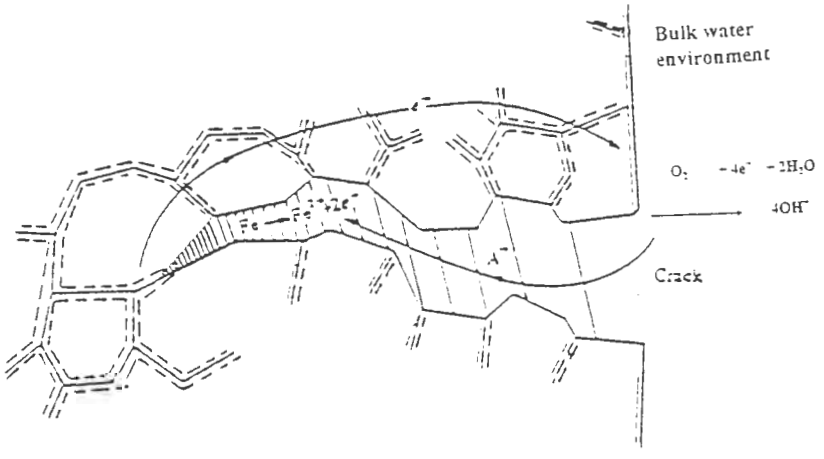

Figure 2.17: A schematic model of the crack propagation mechanism along sensitised grain boundaries (after Weeks[57]).

2.4.2 Strain-assisted active path mechanism

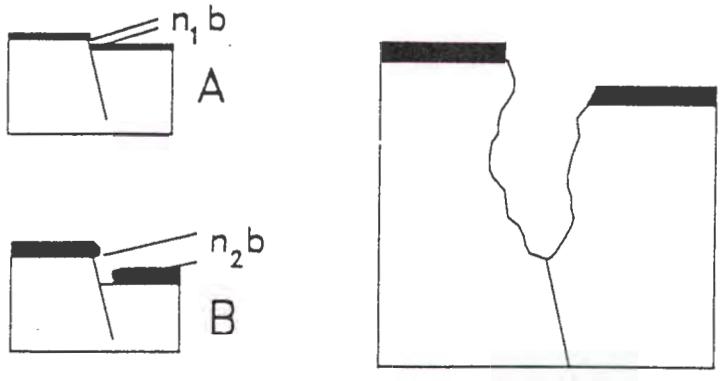

Figure 2.18: Film rupture of a metal with low stacking fault energy. Thin film A ruptures more easily than thick film B (after Kowaka[58]).

The stress concentration effect of a crack or other defect causes a region of plastic deformation. This encourages the accumulation of dislocations which manifest themselves by the appearance of slip steps at the defect. These dislocations disrupt the protective passive film and expose bare metal to the environment, thus initiating a crack[58]. This process is illustrated in figure 2.18

2.4.3 Adsorption Mechanism

This theory proposes that impurity atoms such as hydrogen and sulphur diffuse to the crack tip and become adsorbed to the surface, thus locally weakening the interatomic bonding of the metal[59] (see figure 2.19).

Dislocations initiate and are injected into the metal along the planes of maximum shear stress (i.e. at 45° to the principle tensile stress)[61]. This leads to an incremental crack growth process similar in nature to fatigue crack growth[21].

The propagation rate is controlled by the transport of aggressive species to the crack tip region. Inhibiting ions compete with aggressive species for adsorption sites on the metal surface[60].

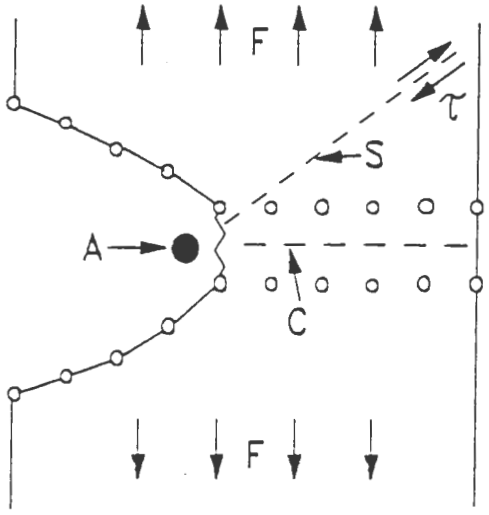

Figure 2.19: Adsorption of atom A at the crack tip causes a weakening of interatomic bonding in the base metal (after Silcock[61]).

2.4.4 Film induced cleavage

This theory attempts to explain transgranular stress corrosion cracking. It is based on the evidence that a spongy non-oxide layer is formed within the cracks, which is a de-alloyed metal with a continually varying composition throughout its thickness. The theory proposes that the presence of this film at a crack tip can modify local deformation processes[62].

2.5 Stress corrosion test methods

Stress corrosion cracking is a complex phenomenon which requires considerable understanding of all factors involved. The purpose of any stress-corrosion testing is to simulate on a small scale the conditions that exist in an engineering application. However, stress corrosion cracking can occur after as little as a few hours of exposure or after years of satisfactory service. This presents difficulties when measuring this phenomenon.

Several loading methods are employed in the study of stress corrosion cracking and the more common ones are dealt with in the following sections. The variation of stress and strain with time to failure is illustrated in figure 2.20.

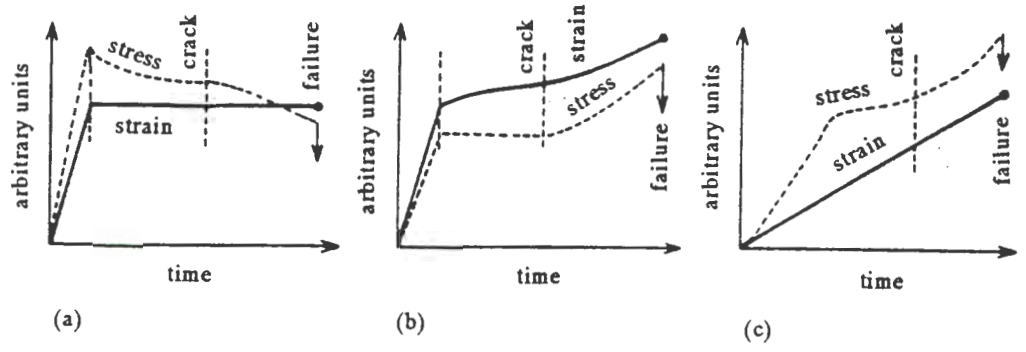

Figure 2.20: The variation of stress and strain during the main test methods is illustrated in these schematic diagrams.
(a) Constant displacement test, (b) Constant load test
(c) Slow strain rate test (after Kowaka[58]).

2.5.1 Constant displacement test

The simplest form of loading is to hold the specimen at a predefined elastic or plastic strain and examine for signs of intergranular attack after a specific time of immersion in the corrosive environment. The constant displacement method commonly uses two specimen geometries for testing, i.e., the bent beam test and the U-bend test. These are illustrated in figure 2.21.

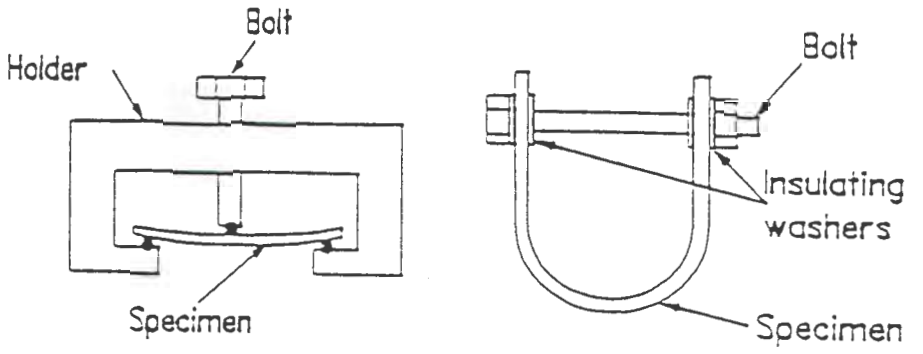

Figure 2.21: The bent beam and U-bend test methods employ specimen statically strained to a predefined deflection and immersed in a corrosive solution (after Logan[63]).

The bent beam test commonly uses three–supports systems[64], in which case the maximum stress is given by :

$$Stress = \frac{6\,Ety}{L^2}$$

where stress is in MPa, E is the elastic modulus in MPa, t the thickness of the specimen in mm, y the deflection in mm and L the distance between the outer supports, also in mm.

The constant displacement test is normally used together with the other SCC test methods. For example Tsuruta and Okomoto[65] used this method together with the constant load test (see section 2.5.2) to investigate the susceptibility to SCC of AISI 304 SS in oxygenated high purity water at temperatures below 240°C. This test revealed the same SCC tendency when compared to the load test under the same conditions.

In another study, Yang et al.[66] compared this method to the slow strain rate test (see section 2.5.3) when investigating the effects of temperature, chloride

content, and dissolved oxygen content on the susceptibility of type 304 SS to SCC. They found the susceptibility to decrease with increasing temperature in the range 200 to 300°C when assessed with the U-bend test, but susceptibility increased up to a maximum at 250°C when assessed by the slow strain rate method.

Yang et al.[67], in a separate study of surface films formed during the testing of specimens, suggested the solution to this mystery. They proposed that the oxide formed on the SS in high temperature water is enhanced in nickel content for SSR test but no significant nickel enhancement occurs in the oxides formed on constant displacement test.

Constant displacement specimens are popular because they are easy to produce and test. High–temperature tests can be conducted in an autoclave without the necessity of sliding seals, which are required for constant load test. However, the disadvantage of this test method is the long time required for a single test and the complex stress profile which makes the analysis of stress difficult.

2.5.2 Constant load test

The tensile specimen is subjected to constant load, usually by suspending a mass from one end, and the time to failure is recorded. Figure 2.22 illustrates the apparatus used with the uniaxial stress: the rod in the beaker is subjected to a constant tensile load while there is a heater at the bottom and a water condenser at the top. The susceptibility to SCC is evaluated from the time to failure and the threshold stress.

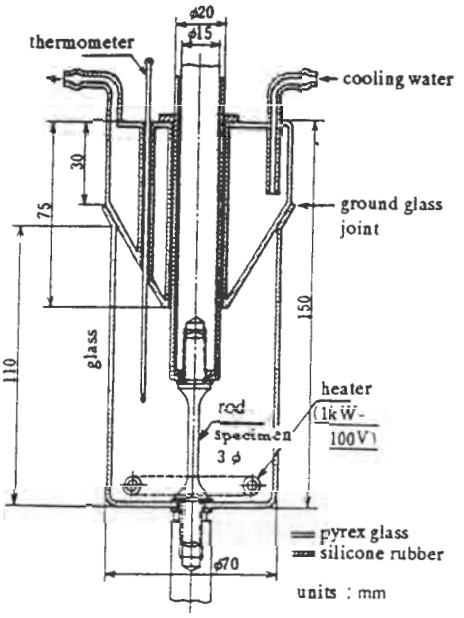

Figure 2.22: Constant-load SCC test equipment (after Kowaka[58]).

These tests are more expensive than the constant displacement test and also suffer from the possibility of inconclusive results if the tests are terminated after some cut-off time without specimen failure. Tokiwai et al.[68] employed the constant load test in the investigation of the critical amount of chloride contamination with varying stress level in air that could cause SCC in sensitised AISI 304 SS. The results showed strong dependence of chloride amount on stress level. They appraised this method's suitability for that task.

2.5.3 Slow strain rate method

In 1961 Nikoforava suggested the original SSRT principle and, subsequently, Parkins and Scully[69] used it extensively. This method gained popularity because it is relatively quick and always results in the failure of the specimen[70]. It is, however, an unusually aggressive method and therefore the results obtained in the SSRT method cannot be extrapolated to true plant conditions[71].

The SSR method is a tensile test whereby the specimen is slowly strained to fracture while in contact with the testing solution. Typically strain rates in the range $10^{-4}s^{-1}$ to $10^{-7}s^{-1}$ are employed. Figure 2.23 shows SSRT equipment and the reference stress-strain curve which can be derived from measurements

in an inert environment. The deviation from unity is used as an indication of the extent of susceptibility.

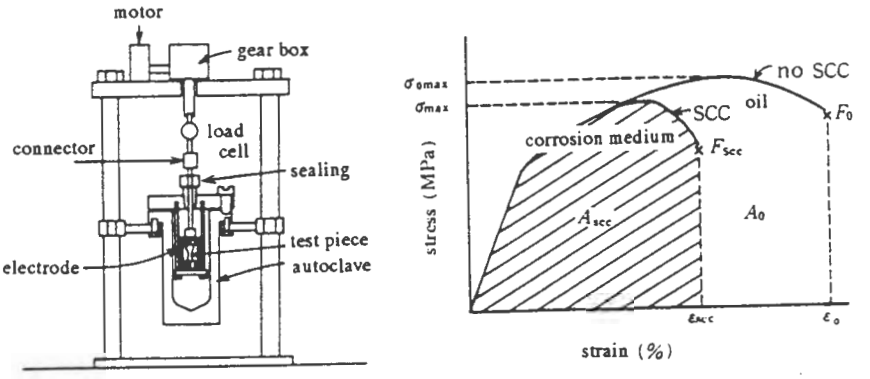

Figure 2.23: SSR test equipment and SSRT sensitivity evaluation (after Kowaka[58]).

Metallography and fractography are always used to verify the presence or absence of SCC after SSRT. Severity of SCC depends on the material / environment parameters and borderline cases between regions of severe SCC and regions where no SCC exist. This makes the interpretation of SCC results difficult. Payer et al.[72] suggested that the appearance of numerous secondary cracks along the gauge length, which must be perpendicular to the applied stress, together with the loss of ductility is a clear indication of the presence of SCC. Figure 2.24 is an illustration of unetched metallographic cross sections after a SSRT. The figure shows a range from clear SCC indication (bottom of the figure 2.24) to clearly lack of SCC (top of the figure 2.24). The lower two micrographs show secondary stress corrosion cracks along the gauge length and perpendicular to the applied stress. The upper two micrographs show penetration not related to SCC; corrosion pits on the upper right and a penetration oriented at 45° to the applied stress on the upper left.

Figure 2.24: Montage of metallographic cross sections through a SS after slow strain rate test showing SCC and nonSCC events (after Payer[72]).

Beavers and Kock[73] conducted a survey on the accuracy of the SSR test based on literature and questionnaires sent to members of the Materials Technology Institute, the National Association on Corrosion Engineers and the American Society for Testing of Materials. The study found that most anomalous results could be attributed directly to inadequate control or measurement of both strain rate and test potential. This has been confirmed by several authors[70-72]. The dissatisfaction with the experimental control has led to some laboratories completely abandoning this method. However this method remains the most extensively used (judging by the volume of publications) in the investigation of SCC, not because of its experimental soundness but for its expediency.

2.5.4 Fracture mechanics testing method

Constant load pre-cracked specimens have been used in SCC studies to determine the threshold stress intensity for environmentally accelerated crack growth. The use of a pre-cracked specimen simplifies the investigation of crack growth phenomena since no initiation process need be considered[73]. Fatigue pre-cracked specimens can be loaded in each of the following three modes:

- constant strain (using wedge opening specimens)
- sustained static load, and
- slow strain rate (usually referred to as rising load tests).

2.5.5 Electrochemical method

SCC occurs in a particular material under specific conditions at a certain potential. This potential can be defined for any combination of a material and circumstances by recording anodic polarisation curves at various sweep rates. The potential at which the current varies most with the sweep rate is that causing SCC[58]. The reason for this is that a low sweep rate allows repassivation, while a high sweep rate does not, and therefore the current at high sweep rate is that for the unprotected substrate.

Another method is to measure the current increase as the specimen is strained rapidly at a fixed potential. The rupture of the passive film is important here. The maximum current density is governed by the relation between the strain rate and the repassivation rate. The electrochemical method is particularly useful in the study of the mechanism involved in the SCC for a specific environment. Steward et al.[74] used this method in the investigation of initiation of microcracks in the intergranular stress corrosion cracking of the sensitised type AISI 304 SS in high–purity oxygenated water at high temperatures. They developed a simple statistical model based on a jump probability to cross a barrier when the crack is advancing in the steel. This model, whereby a crack has a simple probability of

jumping from one grain boundary facet to the next, describes the crack length distribution. It was found that the jump velocity is higher for high temperature than for low temperature.

Chapter 3 EXPERIMENTAL TECHNIQUES

3.1 Materials

3.1.1 Samples

Two classes of stainless steel were investigated. Cromanite™ was supplied by Columbus Stainless, Middelburg, South Africa while type AISI 304 stainless steel certified composition was supplied by local distributors Jackson and Sons of Cape Town. The chemical composition for the two materials is given in Table 3.1 below.

Element	Alloy	
	AISI 304	19105 Cromanite™
Carbon	0.049	0.036
Chromium	19.30	18.091
Nickel	**8.56**	**0.59**
Nitrogen	**0.02**	**0.511**
Manganese	**1.34**	**9.74**
Molybdenum	0.20	0.07
Phosphorus	0.028	0.023
Sulphur	0.0079	0.044
Silicon	0.57	0.004
Copper	0.22	0.08
Cobalt	0.11	0.02
Titanium	0.006	0.003
Vanadium	0.03	0.12
Aluminium	0.007	0.022
Niobium	0.001	0.0070
Iron	balance	balance

Table 3.1 The composition of the alloys used in the study in wt %.

3.1.2 Heat treatment

The two experimental alloys were solution treated at 1075°C for 0.5 hour and water quenched. Whenever a material is used in operation it will invariably be welded, hence a simulation of the weld heat affected zone treatment was performed at 675°C for 1 hour and water-quenched.

3.1.3 Metallography

The optical microscope was used to characterise the microstructure of experimental alloys. Nomarski interference and Bright field employed where deemed necessary. Before microscopy, specimens were mechanically ground finishing with 4000 grit SiC paper and polished using high quality SiO_2 slurry.

The two etching conditions used were:

(1) electrolytic etching at 3V for 35-50 seconds in a 10 % oxalic acid solution at 40°C.
(2) electrolytic etching at 3V for 30-60 seconds in 20 % NaOH at 40°C.

These etchants reveal the grain structure and δ-ferrite respectively. Figures 3.1 to 3.4 give the microstructural features of experimental alloys etched in 10 % oxalic acid solution while figures 3.5 and 3.6 show those etched in 20 % NaOH solution.

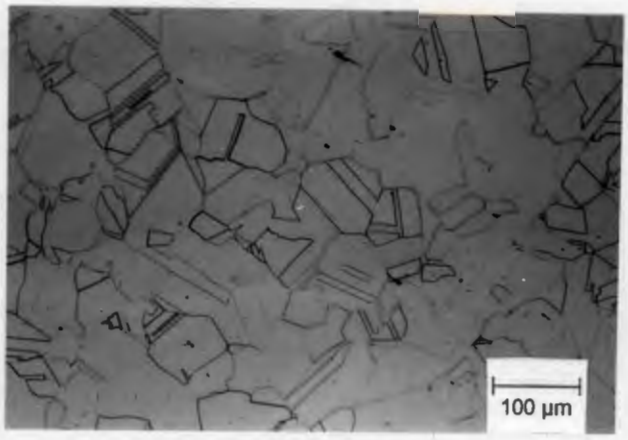

Figure 3.1: The microstructure of Cromanite™ in the solution treated condition, etched in 10% oxalic acid solution.

Figure 3.1 shows fully austenitic microstructure. The austenitic grains are stain-free.

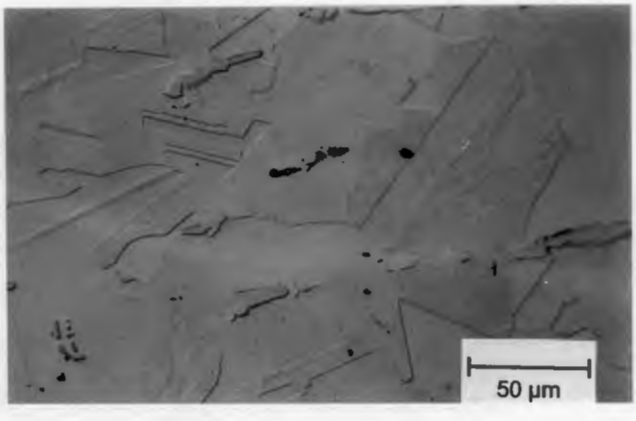

Figure 3.2: The microstructure of AISI 304 in the solution treated condition shows a stepped microstructure of austenite grains according to ASTM A262-91[75].

AISI 304 SS in the solution treated condition (figure 3.2) also shows a carbide-free grain structure.

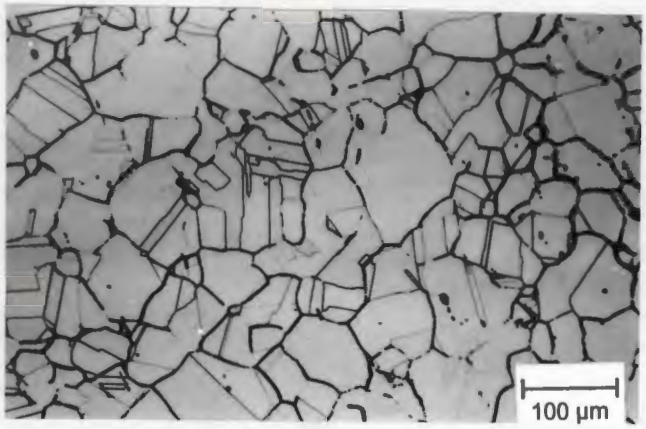

Figure 3.3: The microstructure of Cromanite™ in an aged condition. Electrolytic etching reveals a ditched microstructure according to ASTM A 262-91[75].

The ditched structure shown in figure 3.3 represents a grain structure susceptible to intergranular corrosion attack according to ASTM A 262-91[75] standard test.

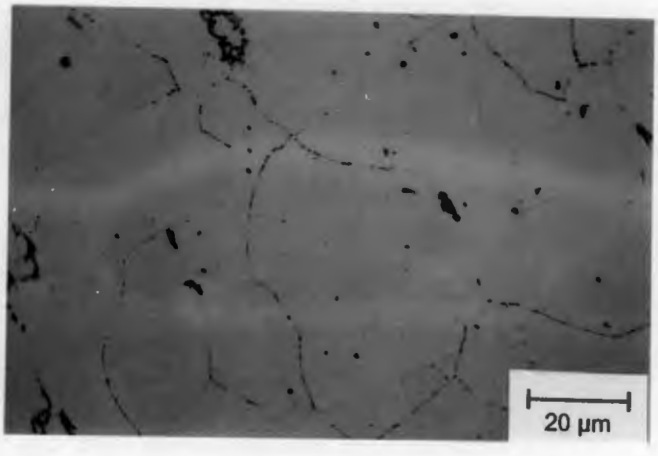

Figure 3.4: The microstructure of AISI 304 in the aged condition shows a dual microstructure of austenite grains according to ASTM A262-91[75].

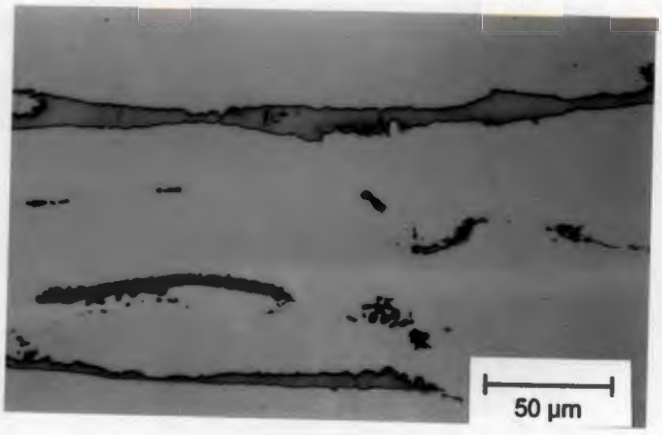

Figure 3.5: The microstructure of AISI 304 in the solution treated condition etched in 20% NaOH to reveal delta-ferrite without affecting grain boundaries.

The microstructure in figure 3.5 shows patches of brown areas of delta-ferrite.

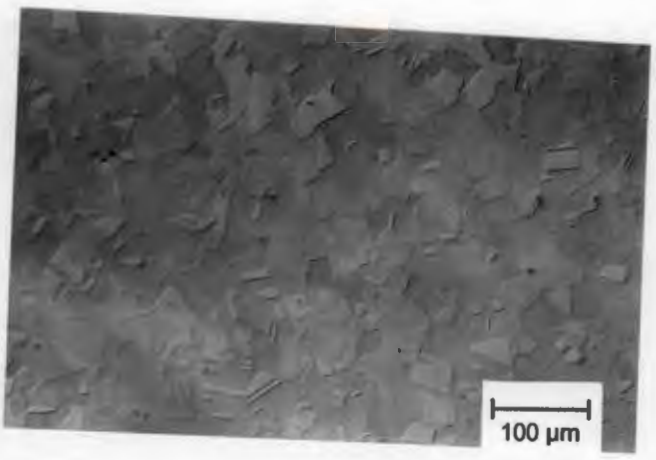

Figure 3.6: The microstructure of the Cromanite™ in the solution treated condition etched in 20% NaOH to reveal delta-ferrite.

There is no evidence of delta ferrite in the microstructure shown in figure 3.6. This demonstrates the superior stabilising effect of nitrogen.

3.2 Corrosion tests

3.2.1 Instrumentation

An Amel system 5000 potentiostat interfaced with the CorrWare for Windows corrosion software package was used to perform corrosion tests. This software package allows a variety of experiments to be done, including potentiostatic, potentiodynamic polarisation, cyclic Voltammogram, galvanostatic, galvanodynamic, impedance, etc. By virtue of the multitasking of the Windows environment, CorrWare can be run in the background allowing the computer to be used for other purposes. The CorrView companion program was used to display, analyse and graph data from Corrware measurements.

A Faraday type cage which shelters the corrosion cell, is provided in order to eliminate electrical noise which may be present in the surroundings. This cage is constructed of wood on the outside and lined with a copper sheeting on the inside. Figure 3.7 shows the instrumentation used during testing.

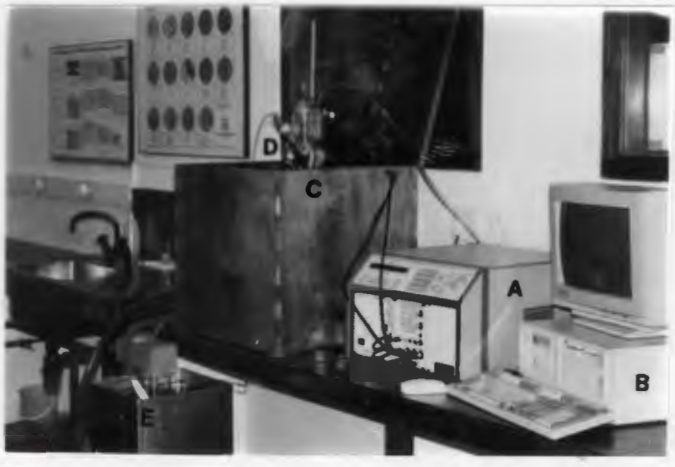

Figure 3.7: Corrosion Instrumentation set-up. (a) AMEL system 5000 Potentiostat, (b) Interface Computer with CorrWare software, (c) Faraday cage housing a test cell, (d) Test cell and (e) Thermo-regulation unit.

3.2.2 Test procedure

Before the commencement of the experiments, it is important to calibrate the system. A test was performed in accordance with ASTM standard G5-78[76] on AISI 430 stainless steel in a 1N sulphuric acid solution. The result of the potentiodynamic test scan indicated a good correspondence with the ASTM standard reference curve.

General corrosion resistance measurements were made on both the alloy samples and their respective heat treated counterparts in accordance with ASTM G5-87[76] and ASTM G61-90[77] standards respectively. A minimum of four scans were performed on a 1 cm^2 rounded specimen mounted in a Teflon specimen holder. The specimen surface was ground to 4000 grit finish. Polarisation tests were performed to determine the characteristic free corrosion behaviour of the experimental alloys in the test environments.

The three different test environments were :

(1) 1N sulphuric acid solution,
(2) 3M NaCl solution, and
(3) 0.05M HCl + 3M NaCl solution.

The corrosion potentials were measured against a saturated calomel reference electrode. The tests were carried out at a scan rate of 0.1667 mV/second in the anodic direction. Argon gas was used to purge and thereby de-aerate the solution for the scan. The solution temperatures were maintained at 30°C using a thermo-regulating unit.

3.2.3 Calculation of corrosion rates

The Stern-Geary equation was used to calculate corrosion rates[78].

$$I_{corr} = \left[\frac{\beta a \beta c}{2.3(\beta a + \beta c)}\right]\frac{1}{Rp} \qquad (3.1)$$

where I_{corr} = corrosion current density in mA/cm^2

βa = anodic Tafel slope in mV/decade

βc = cathodic Tafel slope in mV/decade

Rp = polarisation resistance

The values for βa and βc were obtained from Tafel plots. The Tafel procedure involves polarising the alloy starting at a potential of 150mV below E_{corr} and ending at a potential of 150 mV above E_{corr}. This gives rise to a curve known as an Evans diagram. These curves contain a linear region on a semilogarithmic plot within approximately 50mV of E_{corr}. These regions of linearity are referred to as Tafel regions. It is the slopes of these regions of linearity that produce values for βa and βc.

The value for polarisation resistance is obtained from the slope of the potential-applied current curve as opposed to the potential-current density curve. The slope of this curve at potentials within 10mV of E_{corr} is approximately linear. This slope $\Delta E/\Delta I$, has the units of resistance and represents the resistance within the electrolyte, between the reference and the working electrode.

Once the values for βa, βc and Rp are acquired, I_{corr} could be calculated in mA/cm^2. The conversion of corrosion current density to a corrosion rate in millimetres per year (mmpy) is through equation 3.2.

$$mmpy = \frac{(3.3 \times mA/cm^2 \times E.W)}{d} \qquad (3.2)$$

where 3.3 = metric/time conversion factor
d = density of specimen in grams per cm^3
E.W. = equivalent weight in grams

Stainless steels contain a number of major alloying elements of differing equivalent weights and therefore a calculation must be done to account for these partial contributions of various alloying elements. This is given by equation 3.3.

$$E.W. = \frac{\Sigma((\text{volume element in alloy} \times \text{atomic mass})}{\text{valence}} \qquad (3.3)$$

3.2.4 Sensitisation measurements

The electrochemical potentiodynamic reactivation (EPR) test technique has been developed in an attempt to find a rapid, non-destructive but quantitative method of measuring the degree of sensitisation (DOS) of stainless steels[79].

There are two main variations of this technique, denoted single-loop and double-loop methods. Both involve evaluation of a polarised curve for the material under investigation in a 0.5 M H_2SO_4 with 0.01 M KSCN solution. These methods are both employed in this study.

The single-loop method involves measuring the total charge, Q, in coulombs that flows when a metal is scanned from a passive potential through to the free corrosion potential. If the material is depleted in chromium then the oxide will heal slowly and a larger charge will be required to achieve film healing than that required for the material when not depleted in chromium[80]. The charge Q obtained is then normalised with the grain boundary area (GBA), obtained from the ASTM grain size number[81]. This gives rise to a Pa value, which is a measure of the degree of sensitisation.

$$Pa = \frac{\text{Charge evolved, Coulombs}}{\text{Grain Boundary Area, cm}^2}$$

where the GBA is calculated from the area of the specimen, A_s, and the ASTM grain size number, G, according to the formula :

$$GBA = A_s [5.09544 \times 10^{-3} \exp^{(0.34696G)}]$$ [82]

The inherent assumption in this is that all the corrosion current flowing during the reactivation scan comes from 2μm on either side of the grain boundary[83].

In the double-loop system, the ratio, R_a, of maximum anodic current, i_a and maximum reactivation current, i_r is used. The ratio eliminates the assumption made in calculating the Pa value.

The detailed procedure followed in the double loop method is as follows :

(1) The corrosion potential is determined by immersing the specimen in the 0.5 M H_2SO_4 + 0.01 M KSCN solution for 2 minutes.

(2) The specimen is anodically scanned from corrosion potential to passive region (200mV vs. SCE) at a voltage scan rate of 0.16667mV/second.

(3) It is then held for 2 minutes at a potential of 200mV vs. SCE to accomplish passivation. The current density should be less than 10 μAcm^{-2}.

(4) The scanning is then done in reverse direction (reactivation) at the same rate down to 50mV above the corrosion potential. The charge evolved at this potential is used as the measure of sensitisation.

(5) After the completion of the experiment metallographic inspection is done to analyse the microstructure for the extent of grain boundary attack.

The reactivation polarisation scan causes breakdown of the passive film at sensitised regions in which Cr depletion has occurred. The maximum anodic current, i_a, and maximum reactivation current, i_r, were measured from anodic and reactivation curves, respectively. The reactivation ratio, R_a, is the ratio of maximum anodic current to the maximum reactivation current.

Figure 3.8 demonstrates how the R_a (%) value is calculated.

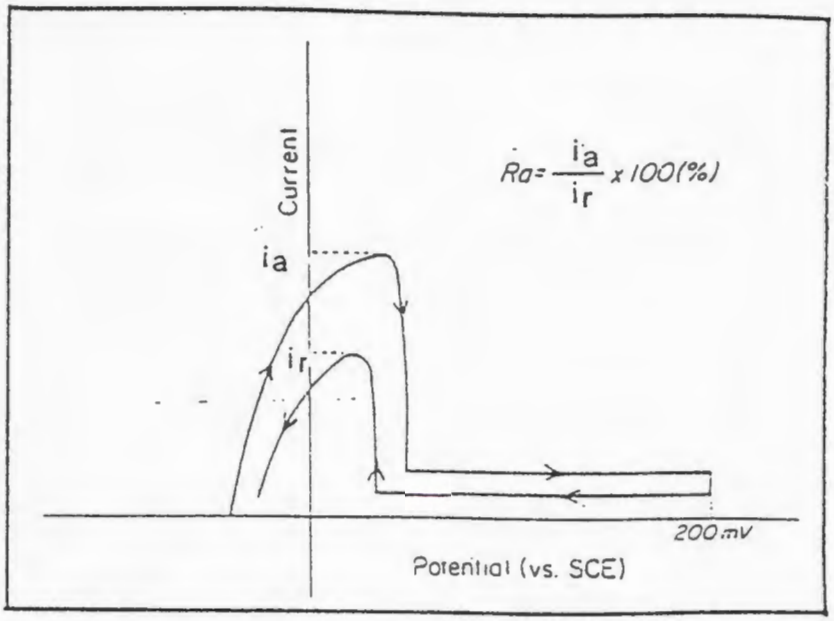

Figure 3.8: Definition of the activation ratio R_a(%) in the EPR technique (after Mozhi[54]).

3.2.5 Grain size measurements

Grain size measurements were done as a requirement for the EPR test, ASTM G108-92[83] standard. Standard test methods for grain size measurements are documented in the ASTM E112-88[81] standard. The linear intercept method was adopted for this study because the alloys under investigation consist entirely of a single phase. This method is accurate to plus or minus half a grain size when necessary statistics have been applied. The detailed procedure followed did not deviate from the ASTM standard E112-88[81]. The grain size measurements results are contained in Appendix A.

3.3 Stress corrosion testing

The two testing methods adopted here are described below.

3.3.1 Slow strain rate testing

The slow strain rate (SSR) test involves straining a tensile specimen, at a uniform extension rate, in a corrosive environment. Strain rate is the most important parameter for tests conducted at open corrosion potential. A nominal strain rate of 3.0×10^{-6} s^{-1} was chosen for the testing because this is the strain rate that produced stress corrosion cracking in type AISI 304 SS[2].

3.3.1.1 Environment

The tests were conducted at open circuit potential on both materials in distilled water, 3 M NaCl, 0.025 M HCl + 3 M NaCl, 0.05 M HCl + 3 M NaCl, 0.15 M HCl + 3 M NaCl and 0.5 M HCl + 3 M NaCl. Distilled water was used in order to avoid the additional complication in the interpretation of SCC process caused by the introduction of different ions. All tests were stabilised at 30°C. The mass lost was monitored as excessive corrosion was observed on Cromanite™.

3.3.1.2 Test Specimen

Slow strain rate (SSR) tests were conducted on round specimens with a gauge length of 15 mm and a diameter of 3 mm, with 6 mm extension to M6 threaded grips. The specimen geometry is shown in figure 3.9.

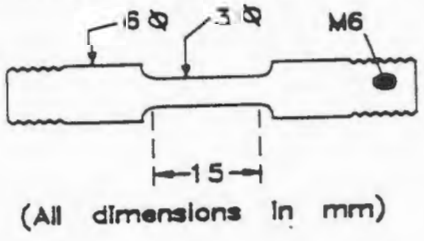

Figure 3.9: Specimen geometry for a slow strain rate tests.

The threaded sections attach to the load frame grips through O-ring seals in the water bath. The specimens were machined from solution treated plates cut into square sections in the rolling direction. The gauge length of the specimen is polished to a 600 grit finish and cleaned in alcohol for 30 minutes before the test.

3.3.1.3 Load Frame

Figure 3.10 shows the test rig used for this investigation. The cross-head speeds necessary for SSR testing are achieved by means of a direct current electric motor which is coupled to two fixed ratio reduction gear boxes followed by a set of toothed belt reduction pulleys. The drive is then passed through a worm and screw gear to the cross-head. Cross-head speed can thus be controlled by a ten turn potentiometer and for this study was held at 4.5×10^{-5} mms^{-1} which gives the required strain rate of 3×10^{-6} s^{-1}. The upper end of the specimen is coupled through a universal joint to the cross-head frame while the lower end is joined via an extension rod to a load cell and rose bearing.

Figure 3.10: Photograph of the slow strain rate rig used in the investigation.
(a): computer interface, (b):load frame, (c):electric motor,
(d):water bath, (e): test cell,(f): potentiostat and (g):control electronics.

3.3.1.4 Test cell

The test cell consists of a polymethyl methacrylate (PMMA) cylinder with a volume of 400 cm^3. This is illustrated in figure 3.11. The specimen passes through O-ring seals in the base of the test cell and in the upper tube, to the threaded grips. The cell has a PMMA lid to limit evaporation and to hold the four high purity graphite counter electrodes. The salt bridge to the reference electrode passes through the side of the test cell and ends 5 mm from the gauge length of the test piece.

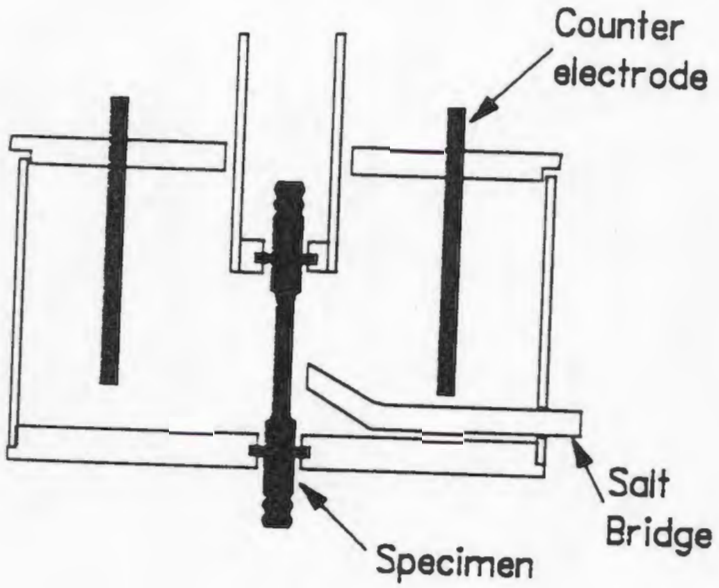

Figure 3.11: Schematic diagram of the test cell design for the slow strain rate tests.

The solution is held in a 6 litre constant temperature water bath. This volume of solution was used to provide a buffer against temperature change and contamination from the anodic dissolution of the specimen. The solution was pumped through silicone rubber tubing into the test cell by a thermo-regulating pumping unit. An aquarium pump is used to continually aerate the test solution in the holding tank.

3.3.1.5 Experimental procedure

The test solution is prepared and placed in the water bath to be heated to the test temperature. The gauge length of the specimen is polished to a 600 grit finish, then cleaned in alcohol. The test specimen is mounted through the O-rings and a small pre-load is applied to remove the slackness in the loading chain. The solution is introduced into the test cell and after the specimen has reached equilibrium (after 30 minutes) the test is started. At the end of the test the specimen is cleaned in diammonium hydrogen citrate to remove any corrosion product.

Fractographic evaluation is conducted in a Cambridge S-200 scanning electron microscope (SEM) to characterise the fracture mode. SEM micrographs of the fracture surface were examined for any intergranular or transgranular fracture origins.

3.3.2 Bent - beam testing

The purpose of any stress-corrosion testing is to simulate on a small scale the conditions that exist in an engineering application. For evaluation of materials for a specific application the testing environment should be the most severe conditions to which the materials would be subjected to in service. However when two materials are compared for relative susceptibility, the test condition chosen must be severe enough to produce varying degrees of cracking in the experimental alloys[84]. The bent-beam test is well suited for establishing the comparative susceptibility of alloys for the relative severity of environments.

The tests, carried out according to ASTM G39-90[84], involved immersion of elastically deformed samples in an aerated solution at room temperature over a period of time, and the time to crack is determined. The cracking time is used as a measure of stress corrosion resistance of the material in the test environment at the given stress level used. The following test conditions were chosen :

Solution	0.05M HCl + 3M NaCl
Sample deflection	1.5 mm
Resultant stress	300 MPa
Maximum period	100 days

3.3.2.1 Sample geometry

The dimensions of the samples used were 25 mm x 127 mm with a thickness of 3 mm. The thickness of the samples, according to ASTM G39-90[84] depends on the mechanical properties of the material. This thickness yields a stress level lower than the yield strength of the experimental alloys.

3.3.2.2 Stressing Jig

The sample is stressed using a load apparatus or jig, and is held in the stressed position throughout the test with the use of the holder. The solution was aerated for the duration of the experiment.

A photograph of the four-point bending stressing jigs used in the study is given in figure 3.12.

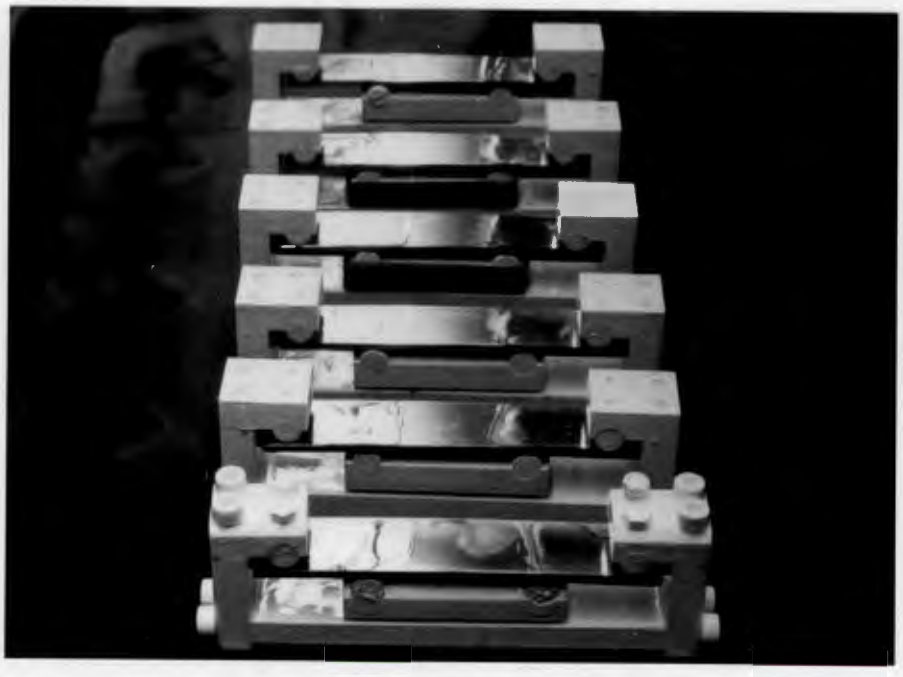

Figure 3.12: A photograph of Stressing jigs fitted with specimens before exposure in the test solution.

The figure shows specimens before immersion in the test solution. The specimens were coated with incralac varnish leaving only the centre part where the applied stress is uniform. Initial problems of crevicing were overcome by coating the holder with epoxy resin.

3.3.2.3 Surface Finish

Smooth surface finish is important in SCC studies otherwise a surface defect might serve as a crack initiation site. The specimens were polished to a 0.25μm finish to remove surface stress raises in accordance with the requirements of ASTM G39-90[84] standard.

Chapter 4 RESULTS

4.1 Materials

4.1.1 General corrosion properties

A solution of 1N sulphuric acid was used in the comparison of the general corrosion properties of the materials. This is given in figure 4.1 below.

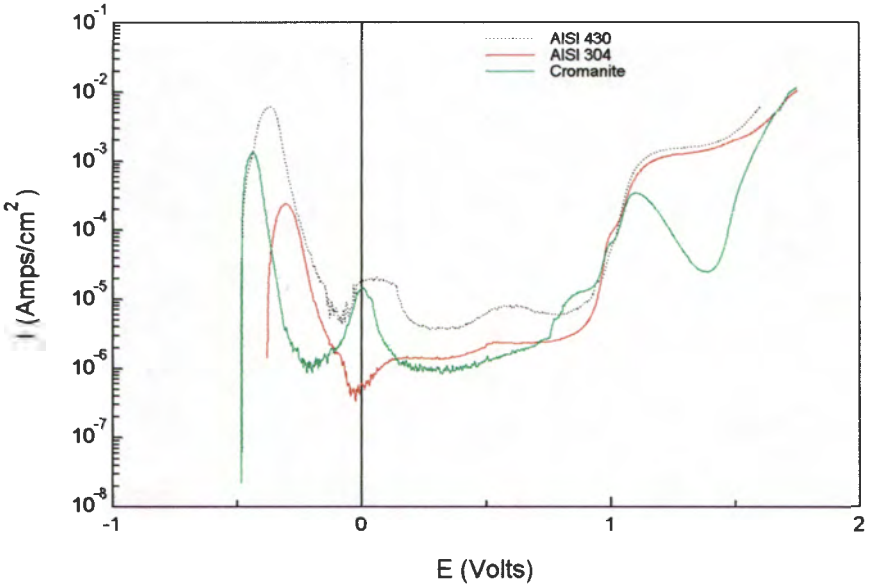

Figure 4.1: Potentiodynamic scans for solution treated samples scans in 1N sulphuric acid.

Figure 4.1 reveals that the behaviour of Cromanite™ and AISI 304 SS samples in 1N sulphuric acid is comparable though the critical current density for Cromanite™ is higher. The scan shows a significantly better corrosion behaviour for austenitic stainless steels, viz. Cromanite™ and AISI 304 when compared with AISI 430 ferritic stainless. The critical current density and passive current density of AISI 430 stainless steel are notably higher when compared to both AISI 304 and Cromanite™. However the potential range at which the SS are passive is the same for all three SS.

Figure 4.2 presents the potentiodynamic scans of aged alloys in 1N sulphuric acid. This figure shows that the stainless property for both materials has been retained in the aged condition, but the passive current density and passive potential range differ significantly when compared with those of the solution treated samples. The general corrosion degradation in the aged condition is similar for both materials although the difference in critical current density for the aged samples has widened.

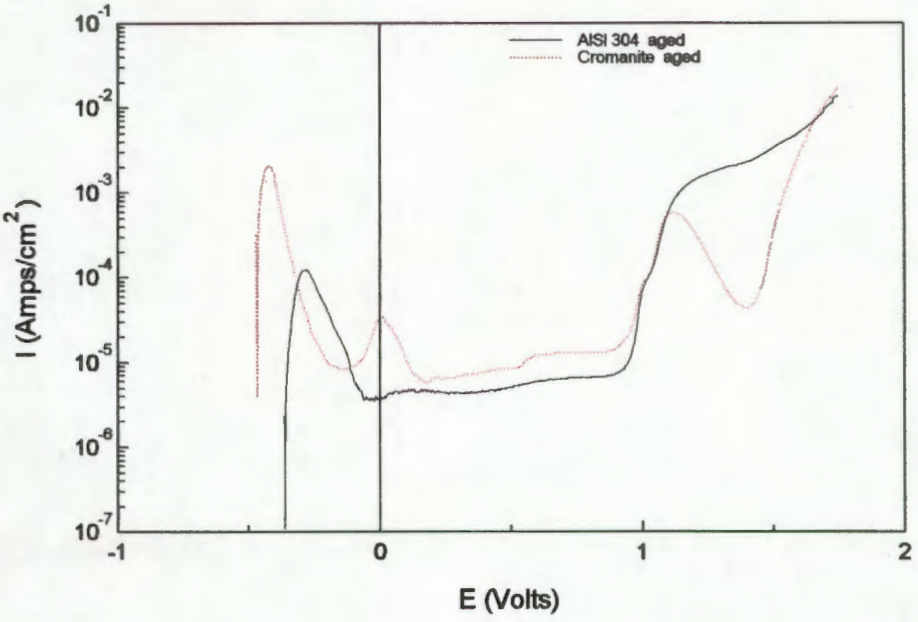

Figure 4.2: Potentiodynamic scans of aged experimental alloys in 1N sulphuric acid.

The corrosion rates computed from Tafel plots are presented in Table 4.1 below.

Alloy	Condition	Corrosion rate ($mmyr^{-1}$)
AISI 304	Solution treated	0.098±0.067
AISI 304	Aged	1.83±0.476
Cromanite™	Solution treated	0.97±0.092
Cromanite™	Aged	2.55±0.959

Table 4.1: Corrosion rates calculated from Tafel plots in 1N H_2SO_4

The corrosion rate measurements were performed in de-aerated 1N sulphuric acid at 30°C at a scan rate of $0.1667 mVs^{-1}$. These measurements show that there is a significant difference in the corrosion rates of AISI 304 SS and Cromanite™. Table 4.1 also shows a higher increase in Cromanite™ corrosion rates for both solution treated and aged specimens when compared to aged AISI 304 SS.

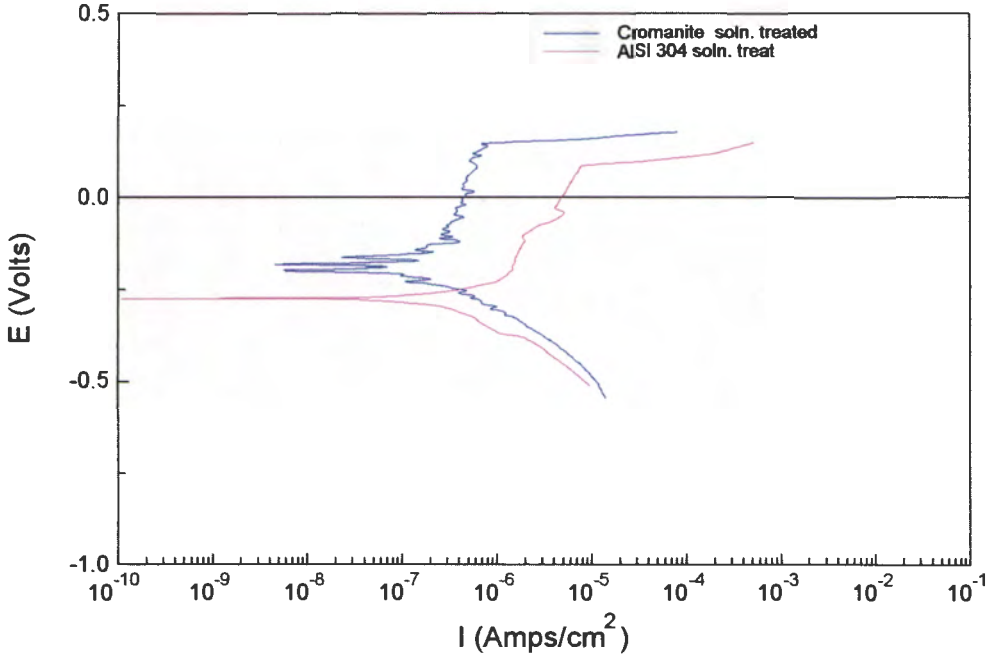

Figure 4.3: Potentiodynamic scan of solution treated specimens in 3M NaCl solution.

Figure 4.3 shows potentiodynamic scans performed in salt solution to compare the corrosion properties of these alloys in this solution. Cromanite™ performs fractionally better than AISI 304 SS as is shown by the higher pitting potential and lower passive current density. It is worth noting that in some cases there was absolutely no difference in pitting potential of the two materials but the results presented are reproducible. However there is a notable shift in corrosion potential, E_{corr}, towards a more active direction in comparison with AISI 304 SS.

The bent-beam tests were carried out in 0.05 M HCl + 3 M NaCl solution. The corrosion rates computed for the experimental alloys from Tafel plots are given in Table 4.2. This table shows that the solution treated Cromanite™ has faster corrosion rates than AISI 304 in the same heat treatment condition. Potentiodynamic scans for this solution are presented in figure 4.4 for both solution treated and aged samples.

Extremely fast corrosion rates were observed for aged Cromanite™, where the specimen was found to be corroding at approximately twice the rate of the aged AISI 304 SS.

Alloy	Condition	Corrosion rate ($mmyr^{-1}$)
AISI 304	Solution treated	4.67±0.934
AISI 304	Aged	7.49±1.489
Cromanite™	Solution treated	5.97±0.740
Cromanite™	Aged	14.95±3.754

Table 4.2: Corrosion rates calculated from Tafel plots performed in a 0.05 M HCl + 3 M NaCl.

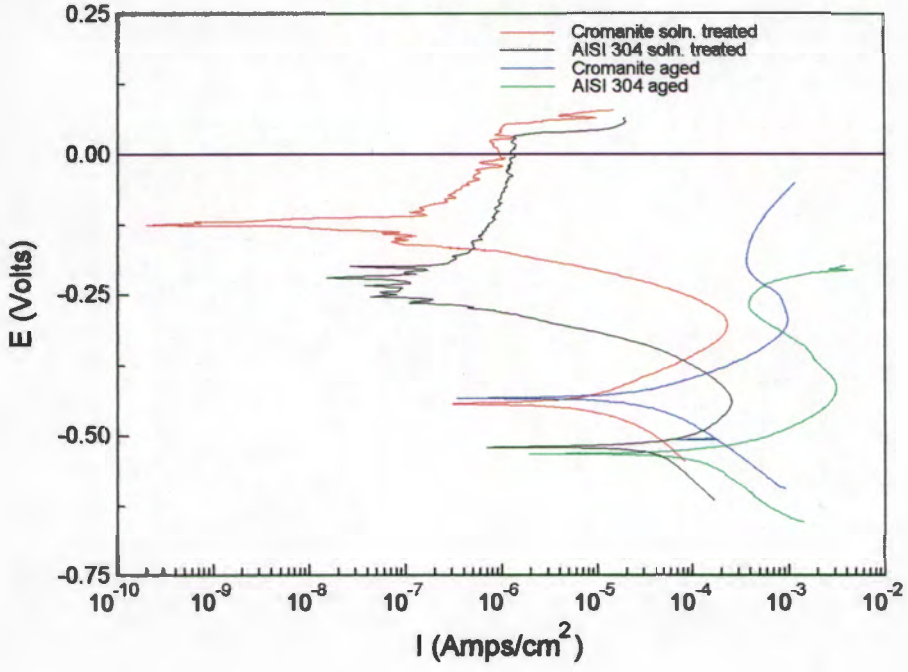

Figure 4.4: Potentiodynamic scans of experimental alloys in 0.05M HCl + 3M NaCl solution.

The solution treated specimens performed equally in this solution as shown in figure 4.4. The pitting potentials and critical current densities for both alloys are very similar with Cromanite™ having an insignificantly higher pitting potential. The aged counterparts both showed active corrosion behaviour in this solution though their corrosion rates differ markedly.

4.1.2 Sensitisation measurements

The heat treatment (675°C for 1 hour) performed on the materials was an attempt to induce sensitisation of the microstructure. The results of EPR scans generated from the two alloys and their aged counterparts are shown in Table 4.3. The normalised charge per unit area values (Pa) from a single-loop method together with the ratio of maximum anodic current (i_a) and maximum reactivation current (i_r), R_a(%), from a double-loop method were computed. These two parameters are used to quantify the degree of sensitisation (DOS). The results of Pa and R_a(%) values shown below are the average of three scans.

Material condition	Pa Single-loop method	R_a Double-loop method
	(Coulomb cm^{-2})	(%)
Cromanite™ soln. treated	0.0478	4.58
Cromanite™ aged	0.4595	36.68
AISI 304 soln. treated	0.0408	2.42
AISI 304 aged	0.2078	16.41

Table 4.3: EPR test results computed from the EPR scans.

The Pa and R_a(%) values found for Type AISI 304 SS are of similar magnitude to those reported by other workers elsewhere[82,85-86].

The classification scheme for the Pa values based on ASTM G108-92[83] is given in table 4.4 below:

Pa value	General Interpretation
< 0.10	Unsensitised microstructure; no pitting
0.10 - 0.4	Slightly sensitised microstructure; pitting and limited intergranular attack
> 0.4	Sensitised microstructure; pitting and attack of entire grain boundaries

Table 4.4: Interpretation of EPR values.

The total charge evolved during the reactivation scan was captured directly using the testing equipment. The anodic and reactivation polarisation scans (double-loop method) produced during the EPR test are given in appendix B.

The plot of potential versus the charge in Coulombs evolved (single-loop method) from the sample during the scans for the solution treated samples and their aged counterparts is given in figure 4.5.

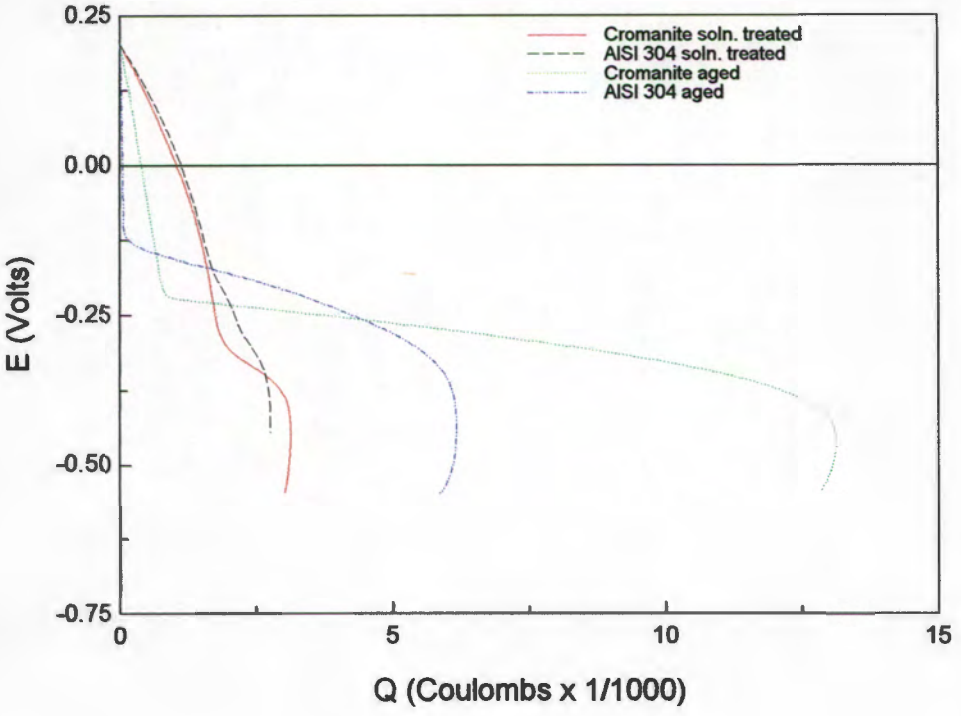

Figure 4.5: EPR scans for experimental alloys and their aged counterparts .

The notable feature about the figure above is the amount of charge which evolved in the aged Cromanite™ specimens. The R_a(%) value obtained for this scan was 36.68% with a Pa value greater than 0.4 Ccm^{-2} which, according to Table 4.4, represents a heavily sensitised microstructure with pitting and severe grain boundary attack.

The behaviour of Cromanite™ solution treated samples was comparable to that of the AISI 304 SS solution treated specimens. The two specimens showed very low values of both R_a(%) and Pa which represent unsensitised stain–free microstructures. The R_a(%) values found by other workers for type AISI 304 sensitised at 650°C for 1 hour vary over the range of 15–25.0%[85].

After completion of the EPR test, the specimens were etched in 10 % oxalic acid solution to examine the microstructure. This was necessary to confirm sensitisation in all cases except for aged Comanite™ where the specimen etched automatically during the EPR test. The microstructures for solution treated samples resembled those originally etched in 10% oxalic acid solution (see figures 3.1 and 3.2). Those for aged samples are given in figures 4.6 and 4.7.

The R_a(%) and the Pa values found for AISI 304 in the solution treated condition were the lowest found for the two materials. However it should be noted that the values recorded in table 4.3 are average values; in some cases Cromanite™ did achieve some values lower than that of AISI 304 in the solution treated condition.

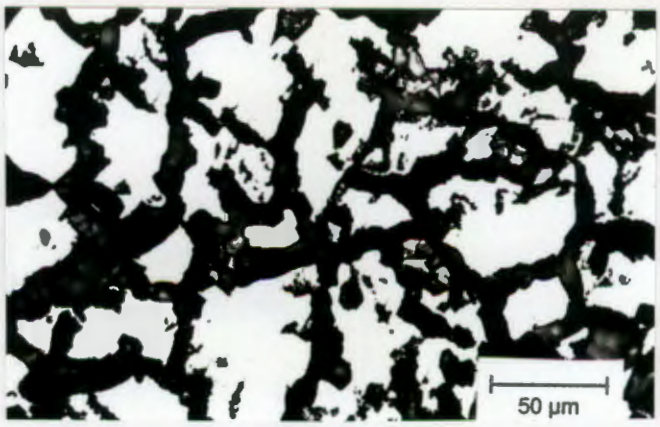

Figure 4.6: The microstructure of aged Cromanite™ after an EPR test.

The high values of Pa and R_a(%) attributed to this microstructure were the results of pitting and severe grain boundary attack.

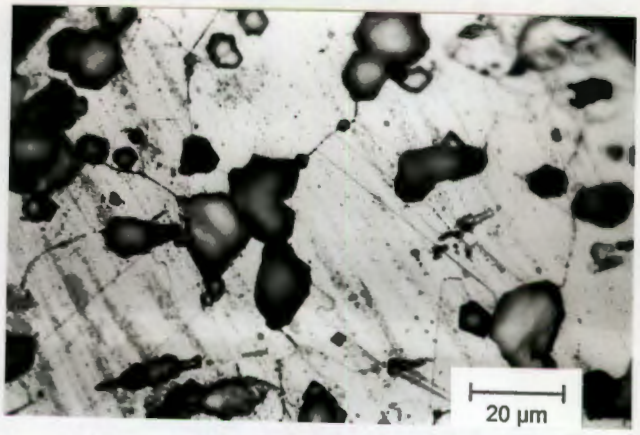

Figure 4.7: The microstructure of the aged AISI 304 stainless steel etched in 10 % oxalic acid solution.

Figure 4.7 shows that the Pa value for aged AISI 304 resulted from the grain boundary attack. Whilst the corrosion rates for AISI 304 in the aged condition and Cromanite™ in the solution treated condition are close to one another (see Table 4.2), their Pa and R_a(%) values clearly differentiate between these alloys. The microstructure also confirms this difference in values.

When the microstructure of aged AISI 304 is compared with aged Cromanite™ (see figure 4.6), it is clear that aged AISI 304 performs significantly better than aged Cromanite™. The R_a(%) value of aged Cromanite™ is more than twice that of aged AISI 304 stainless steel.

4.2 *Stress corrosion properties*

4.2.1 Slow strain rate tests

These tests were only conducted in solution treated samples. This was necessary because of poor mechanical properties of aged Cromanite™. This made SSRT inappropriate method as it relies on the ductility of the material to be reproducible among the specimens on the same environment.

4.2.1.1 Mechanical properties

The Slow Strain Rate (SSR) engineering stress versus engineering strain curves for Cromanite™ and AISI 304 materials tested in 3M NaCl solution containing different concentrations of hydrochloric acid at open circuit potentials are given in figure 4.8 and figure 4.9 respectively.

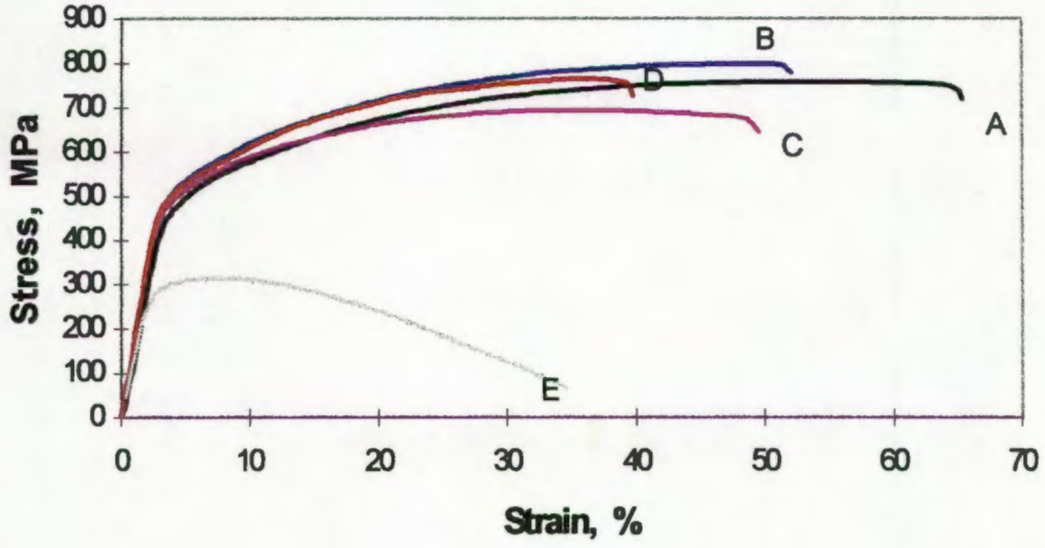

Figure 4.8: The SSR stress vs. strain curves for Cromanite™ material tested on open circuit potential at temperature of 30°C.
A : distilled water, B : 3 M NaCl, C : 0.05 M HCl + 3 M NaCl,
D : 0.15 M HCl + 3 M NaCl, E : 0.5 M HCl + 3 M NaCl

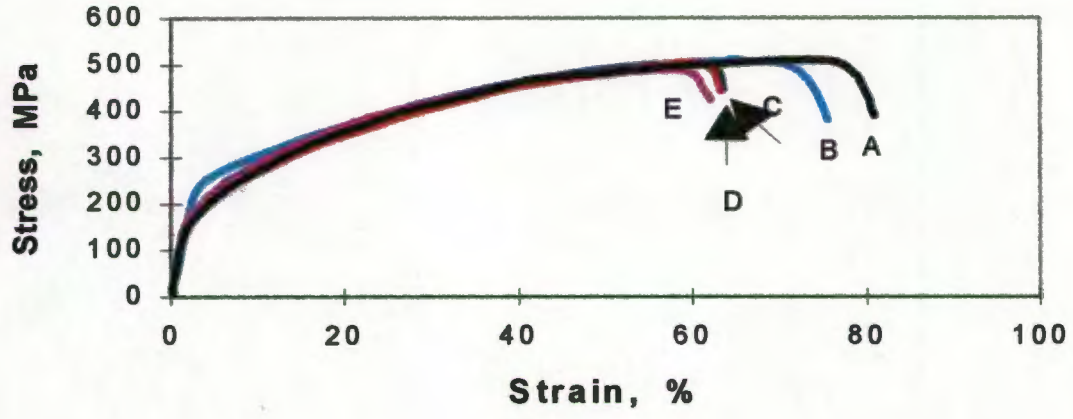

Figure 4.9: The SSR stress vs. strain curves for Type AISI 304 material tested on open circuit potential at 30°C.
A : distilled water, B : 3 M NaCl, C : 0.05 M HCl+3 M NaCl,
D : 0.15 M HCl + 3 M NaCl, E : 0.5 HCl + 3 M NaCl.

The two figures show a marked difference in the mechanical properties of the materials under investigation. The Cromanite™ material tested in distilled water has a UTS of 780 MPa and a proof stress of 500 MPa with a 60 - 66 % maximum elongation. On the other hand AISI 304 material has a UTS of 500 MPa and a proof stress of 264 MPa with a 70-77 % maximum elongation.

The relative effect of the various test conditions can be illustrated by normalising the results with respect to the inert environment, in this case distilled water, to obtain SCC susceptibility indexes (UTS_N, El_N, RA_N). In this way a value of 1 represents no change as a result of the environment while a value less than one indicates a degradation in mechanical properties. The results are shown in Tables 4.5 and 4.6.

Test conditions	Ultimate tensile strength MPa	Maximum elongation %	Reduction of area %	UTS_N	EL_N	RA_N	Mass loss %
Water	779.45	65.13	62.97	1.00	1.00	1.00	0.00
3M Cl^-	779.21	51.95	55.73	1.00	0.80	0.88	0.11
0.05 M H^+ + 3.5 M Cl^-	778.23	42.33	46.43	1.00	0.73	0.74	0.55
0.15 M H^++ 3.5 M Cl^-	700.24	47.51	N/A	0.86	0.65	N/A	2.01
0.5M H^+ + 3.5 M Cl^-	300.43	35.01	N/A	0.37	0.54	N/A	10.43

Table 4.5: Stress corrosion cracking test results for Cromanite™

Test conditions	Ultimate tensile strength MPa	Maximum Elongation %	Reduction of area %	UTS_N	EL_N	RA_N	Mass loss %
Water	512	77.93	69.25	1.00	1.00	1.00	0.00
3M Cl^-	500.01	72.19	62.20	0.98	0.87	0.93	0.00
0.05 M H^++ 3.5 M Cl^-	502.03	65.31	49.02	0.98	0.79	0.70	0.09
0.15 M H^++ 3.5 M Cl^-	504.12	64.89	49.10	0.98	0.79	0.70	0.12
0.5 M H^+ + 3.5 M Cl^-	478.2	63.20	48.09	0.93	0.77	0.69	0.19

Table 4.6: Stress corrosion cracking test results for AISI 304 stainless steel.

4.2.1.2 *Fractography*

4.2.1.2a Distilled water

The fracture surface micrographs for both materials tested in distilled water are presented in figure 4.10. They both show classical ductile failure with shear lips accounting for about half of the fracture surface. Fracture surfaces for both materials exhibit a much greater reduction in area relative to those tested in more corrosive environments.

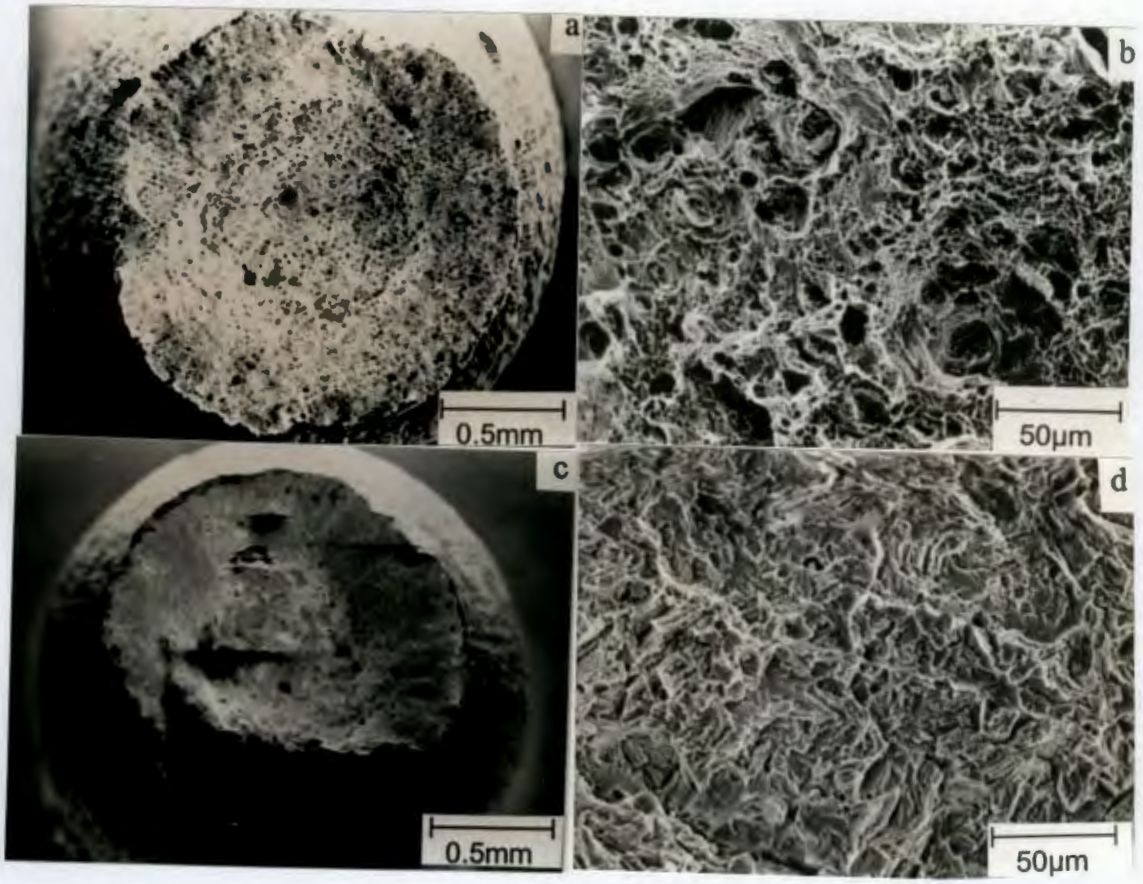

Figure 4.10: Material specimens tested in distilled water at 30°C.

(a) AISI 304 illustrating the ductile fracture surface with pronounced shear-lips.

(b) High magnification for AISI 304 showing a rough fracture surface.

(c) Cromanite™, showing ductile fracture surface.

(d) High magnification for Cromanite™ showing a rough, uneven fully ductile fracture surface.

4.2.1.2b Salt solution (3M NaCl)

When tested in 3 M NaCl AISI 304 exhibits (figure 4.11a) a typical ductile mode of failure. Closer examination of this failure indicates void coalescence (figure 4.11b) as the initial failure mode.

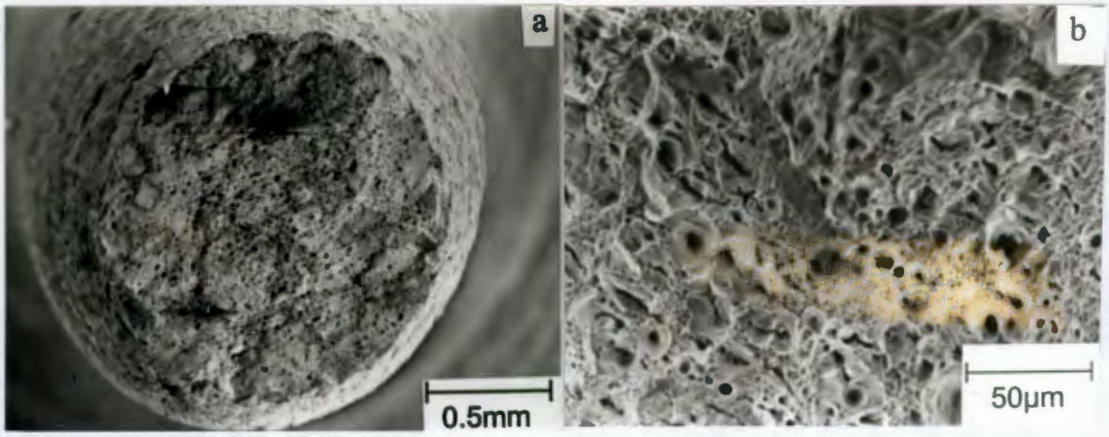

Figure 4.11: AISI 304 specimens tested at open circuit potentials in a 3 M NaCl solution. (a) AISI 304, shows a reduced fracture surface area indicating a ductile mode of failure. (b) Higher magnification of AISI 304.

The fracture surface of Cromanite™ in the same solution is characterised by distinctive branched cracks which is an indication that the material suffered from stress corrosion cracking in this solution. The cracks covered more than half of the fracture surface area as shown in figure 4.12a and b. The specimen showed secondary cracks (figure 4.12c) along the gauge length which were observed to be perpendicular to the applied stress. This is shown in figure 4.12d which is a transverse section through this specimen. The presence of all these is regarded as a clear indication of SCC[72].

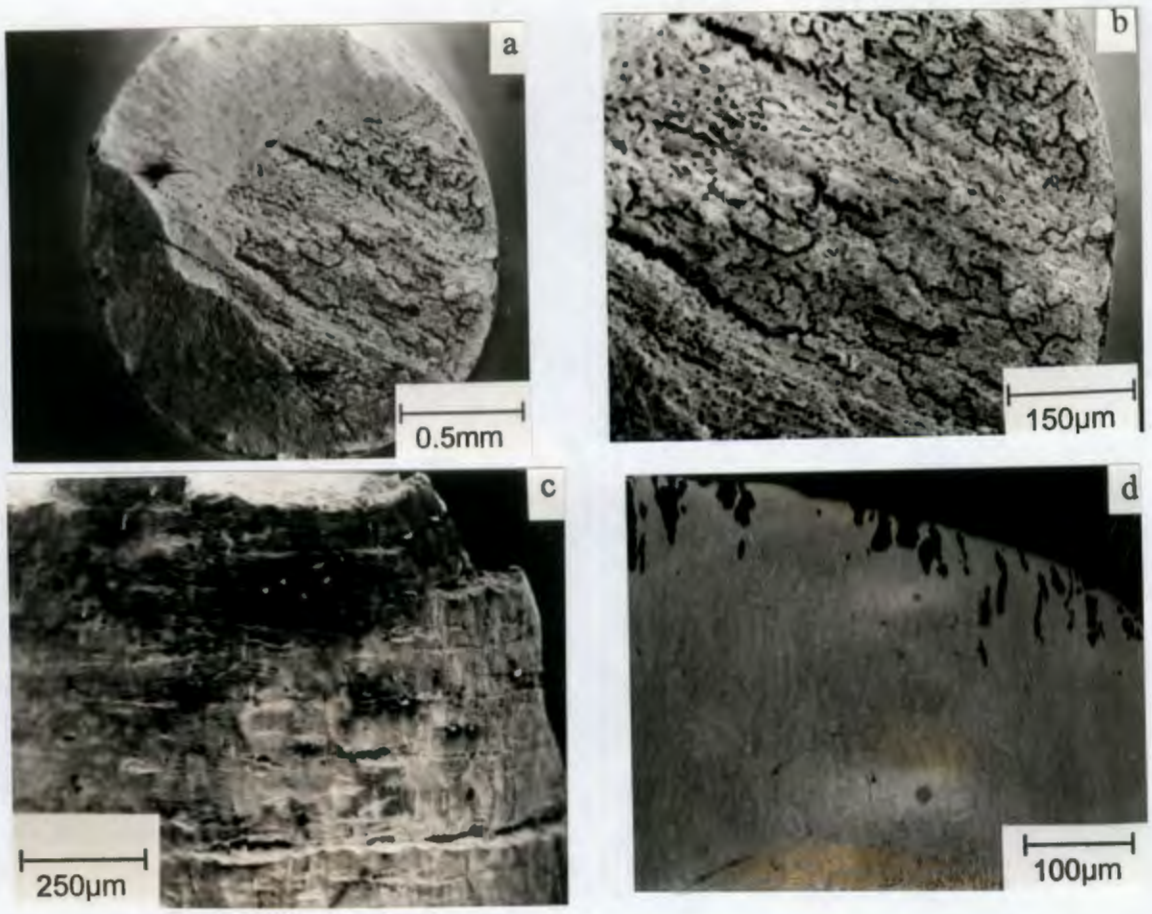

Figure 4.12: Cromanite™ specimens tested at open circuit potentials in a 3 M NaCl solution. (a) Multiple cracking on the fracture surface of the specimen™. (b) A higher magnification of stress corrosion cracks. (c) Secondary cracking along the gauge length. (d) Transverse section through this specimen.

4.2.1.2c 0.05M HCl + 3M NaCl solution

Under these conditions AISI 304 shows a heavily sheared fracture surface with the first appearance of stress corrosion cracking in this material. Figure 4.13a shows the fracture surface of AISI 304 specimen tested at 0.05M HCl + 3M NaCl. The surface is uneven and has a single characteristic branched crack. The higher magnification micrograph (figure 4.13b) shows the branching nature of this crack. The cracking of the specimen along the gauge length (figure 4.13c) together with the characteristics of these secondary cracks (figure 4.13d) is an unambiguous indication of SCC[72].

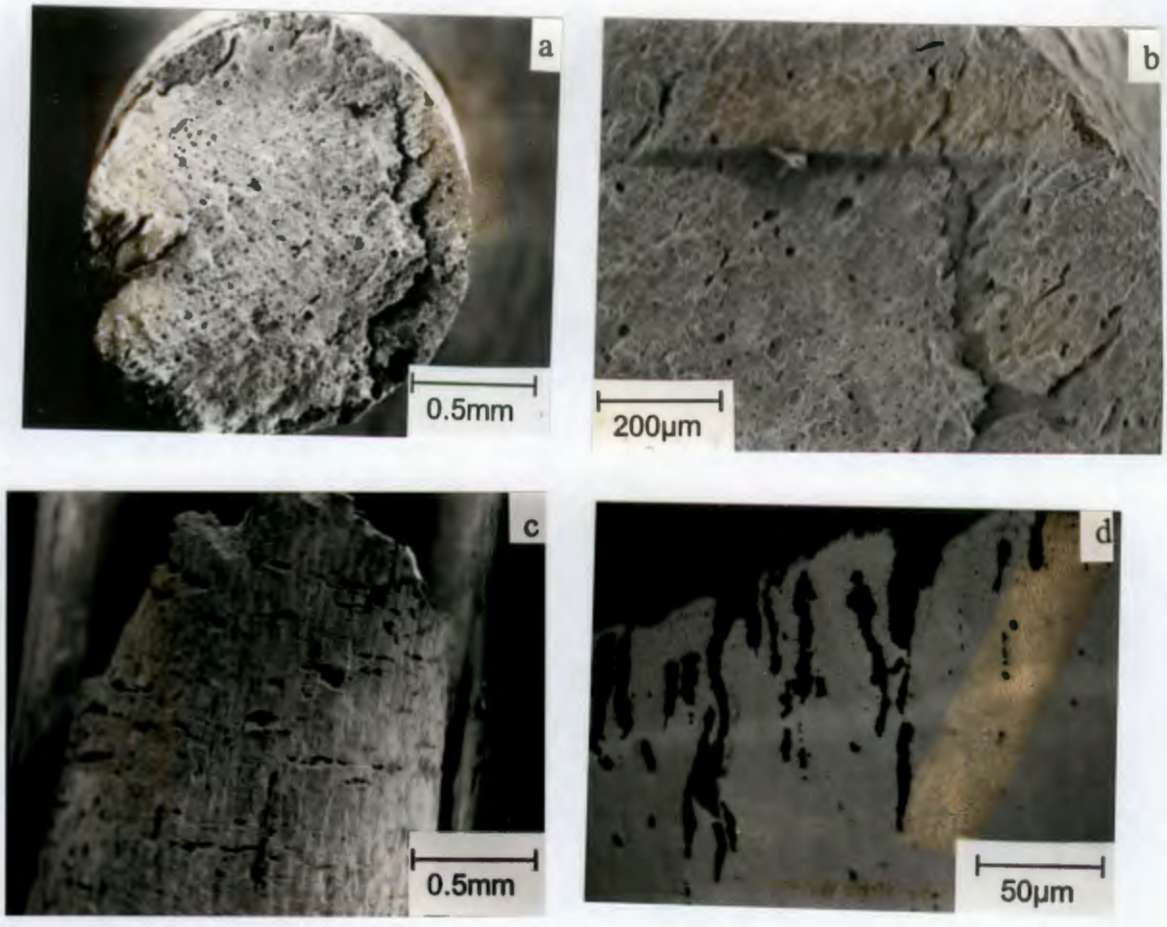

Figure 4.13: AISI 304 SS samples in 0.05 M HCl + 3 M NaCl solution at E_{corr}.
(a) AISI 304 SS shows an irregular sheared fracture surface with the first appearance of stress corrosion cracking in this material.
(b) The higher magnification of this specimen shows the morphology of the crack.
(c) Secondary cracking along the gauge length of AISI 304 specimen.
(d) Transverse section of the specimen shows that these secondary cracks are perpendicular to the applied stress.

Figure 4.14a shows the fracture surface of Cromanite™ which has the main stress corrosion crack as well as other stress corrosion cracks running parallel throughout the surface of the specimen. The specimen shows even more pronounced cracking at higher magnification (shown in figure 4.14b for this material).

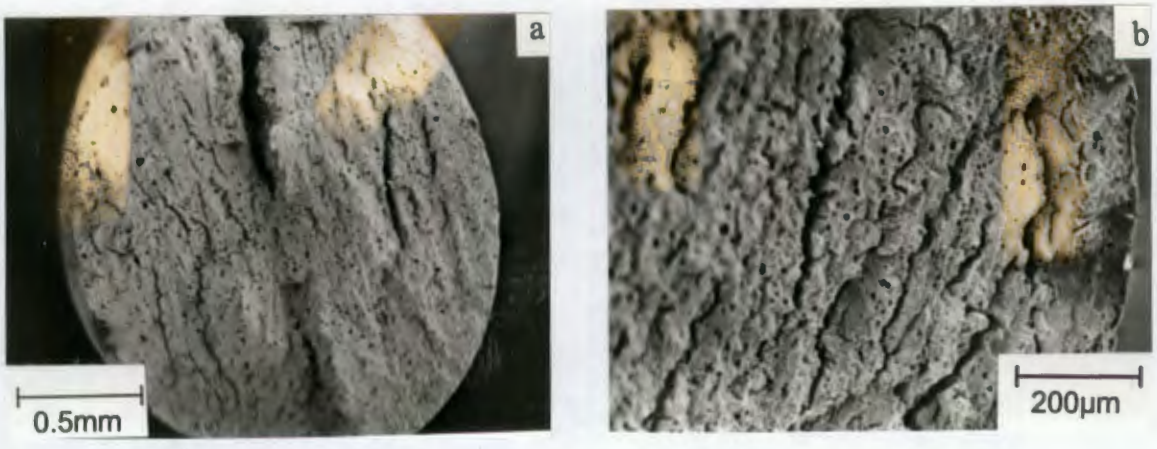

Figure 4.14: Cromanite™ tested in 0.05 M HCl + 3 M NaCl solution at E_{corr}.
(a) Cromanite™ specimen shows a relatively flat fracture surface with single macroscopic crack surrounded by multiple parallel microscopic stress corrosion cracks. (b) Higher magnification of these microscopic cracks.

4.2.12d 0.15 M HCl + 3M NaCl solution

Tests conducted at this acid concentration in Cromanite™ specimens showed significant mass loss, which resulted in a reduction in thickness along the gauge length as a result of high corrosion rates. The RA_N (see Table 4.5) values for Cromanite™ could not be calculated for this reason.

Figure 4.15 contrasts both Cromanite™ and AISI 304 SS specimens after a slow strain rate test. It is evident from this test that AISI 304 has superior corrosion properties to Cromanite™ in this solution. Considerable material has been lost from the gauge length of Cromanite™ specimen.

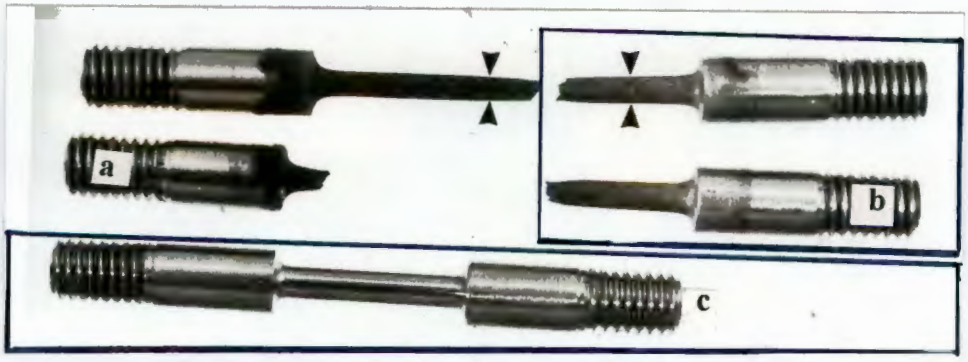

Figure 4.15: Materials specimens tested in 0.15 M HCl + 3 M NaCl at E_{corr} at 30°C (a) Cromanite™ (b) AISI 304 (c) fresh specimen

Figure 4.16 shows AISI 304 SS fracture surface which is dominated by the presence of brittle areas. Cracking started on the edges of the specimen; however, no single crack extended along the entire surface area. Cromanite™ failed due to rapid thinning of the gauge length, hence stress was unable to play any role..

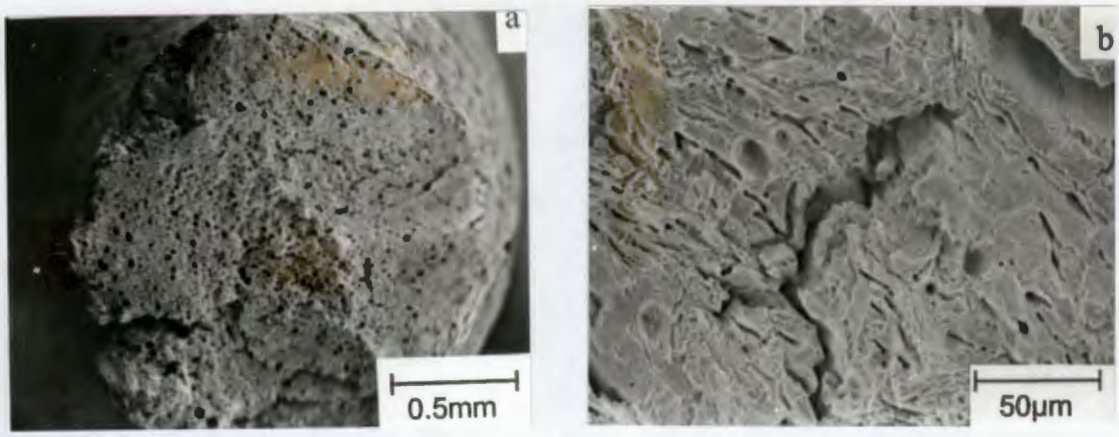

Figure 4.16: AISI 304 tests conducted at 0.15M HCl + 3M NaCl at open circuit potentials. (a) AISI 304 showing a featureless specimen with cracking starting from the edges of the specimen. (b) A higher magnification of this specimen showing the morphology of the stress corrosion cracking.

4.2.1.2e 0.5 M HCl + 3M NaCl solution

Table 4.5 shows a mass loss of 10.43% for Cromanite™ in this solution. Figure 4.17 shows marked thinning of Cromanite™ specimen when compared to both AISI 304 and a fresh specimen. The specimen failed by fast corrosion rates and once more stresses had no time to play any role.

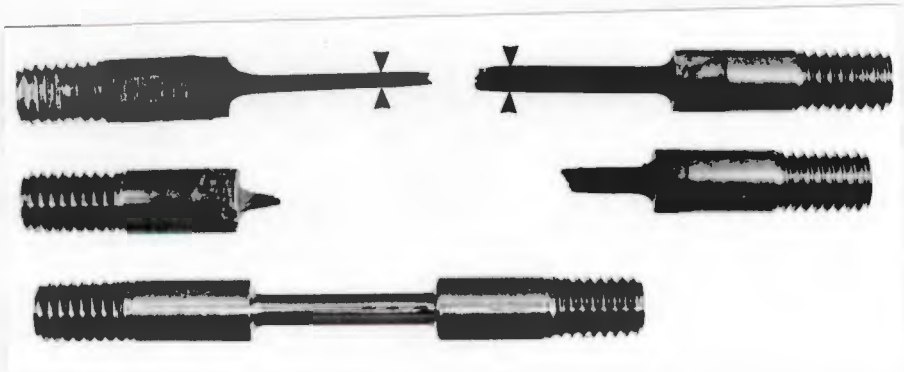

Figure 4.17: Materials tested at 0.5M HCl + 3M NaCl showing marked thinning of Cromanite™ when compared to AISI 304 (a) Cromanite™ (b) AISI 304 (c) fresh specimen

The most remarkable feature about the fracture surface appearance of AISI 304 SS in this solution (figure 4.18a) is the absence of shear lips. The fracture surface is flat with some brittle sites on the edges of the specimen surface. The characteristic branching of stress corrosion cracks is observed in this material at high magnification (shown in figure 4.18b). Pronounced secondary cracking was also observed in this solution. The mass loss as a result of fast corrosion rates is exceptionally low for AISI 304 SS (see Table 4.6).

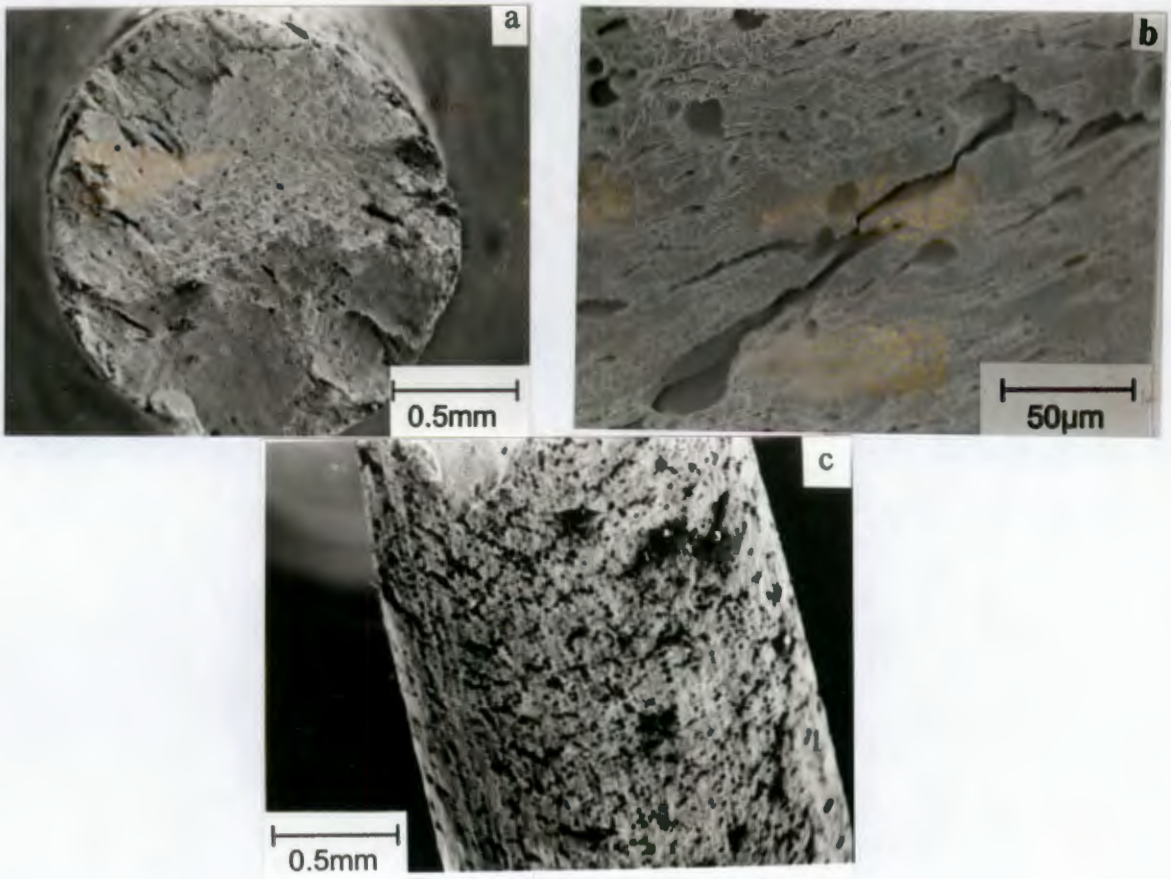

Figure 4.18: AISI 304 specimens tested in 0.5M HCl + 3M NaCl at open circuit potentials.

(a) A featureless fracture surface characterised by a huge single crack which extends along the entire fracture surface.

(b) A higher magnification of the crack from the above specimen.

(c) Major secondary cracking along the gauge length of the specimen.

4.2.2 Bent - beam test results

Elastically deformed bent-beam specimens were immersed in an aerated solution of 0.05M HCl + 3M NaCl solution at room temperature for a maximum period of 100 days. The materials were tested in both solution treated and aged condition. Three samples of each were tested and the time to crack was used as a measure of the susceptibility to stress corrosion cracking. The potentiodynamic scans of all samples tested in this solution have been given in figure 4.5.

4.2.2.1 Solution treated samples

Figure 4.19 gives the bent beam microstructure results for both Cromanite™ and AISI 304 stainless steels in the solution treated condition.

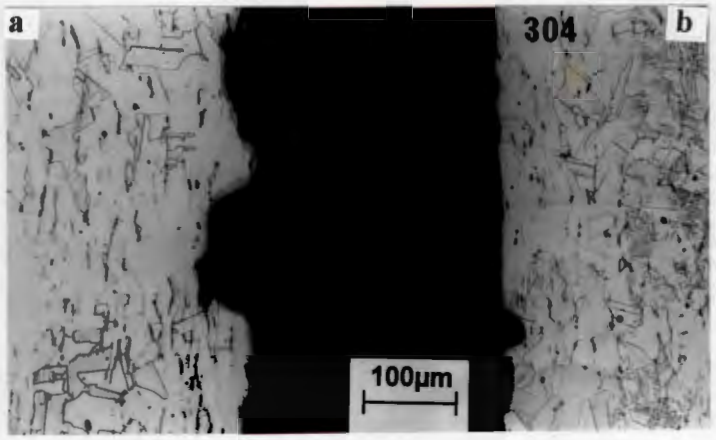

Figure 4.19: Cross section through the specimen after 100 days of immersion.
(a) Cromanite™ (b) AISI Type 304 stainless steel

No evidence of cracking was observed for either material in the solution treated condition. However it is clear from the micrograph that Cromanite™ suffered more from general corrosion after 100 days. The tests discontinued after 50 and 75 days showed the occurrence of general corrosion but no cracking.

4.2.2.2 Aged samples

The tests were discontinued for evaluation for cracks at 25, 50, and 75 days. Cracking was first observed in aged Cromanite™ after 25 days. Figures 4.20 to 4.22 present results for both Cromanite™ and AISI 304 stainless steel samples in the aged condition, at various periods of exposure.

Figure 4.20 shows intergranular cracks in Cromanite™, seen under an optical microscope.

Figure 4.20: Cromanite™ after 25 days of exposure.

One of the three specimens cracked after this period. It is evident from the depth of these cracks that they have propagated in the material though they remain shallow.

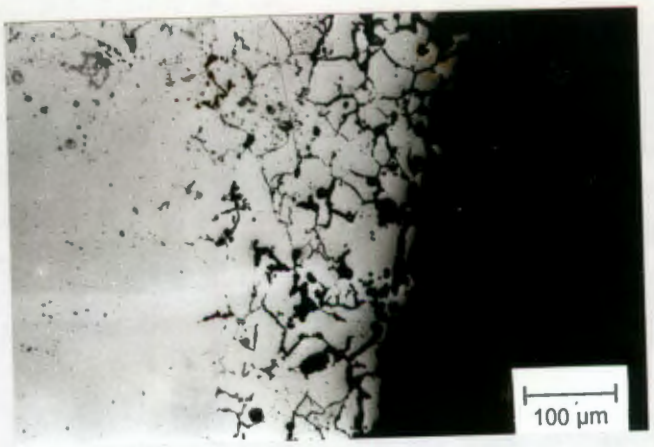

Figure 4.21: Cromanite™ after 50 days of immersion.

All three samples had cracked at the end of this period. Cromanite™ tests were discontinued after 50 days (see figure 4.21) but testing on aged AISI 304 stainless steel continued since cracks had not been observed after 25 and 50 days. Figure 4.22 presents the microstructure of aged AISI 304 after a period of 75 days.

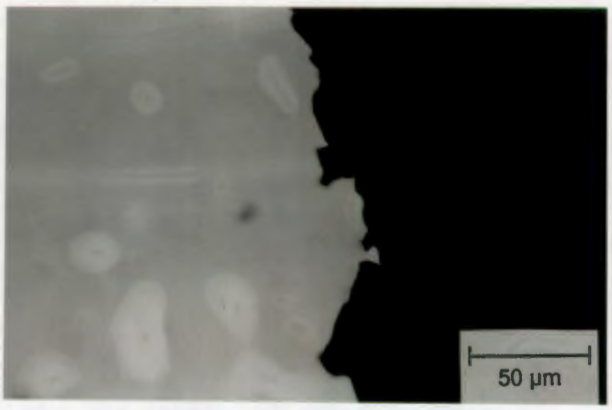

Figure 4.22: AISI 304 stainless steel in the aged condition after 75 days.

All three specimens showed no evidence of cracking at the end of this period.

Chapter 5 DISCUSSION

5.1 Materials

5.1.1 General Observations

The materials were etched in two etchants for microstructural observation. 10 % oxalic acid solution was used to reveal the grain structure while 20% NaOH solution revealed the delta-ferrite without affecting the grain boundaries. The oxalic acid etch is analogous to ASTM A262-91[75] Practice A, where it is used for detecting the susceptibility to intergranular corrosion. Susceptibility to intergranular attack of a microstructure in this test is associated with the precipitation of chromium carbides or nitrides at the grain boundaries. These specimens are identified by means of their etched microstructure which is classified as step, dual and ditched structures.

The microstructure of Cromanite™ (see figure 3.1) is classified as a step structure. There are no ditches at the grain boundaries. It can be concluded that the microstructure is immune to intergranular corrosion attack. However, on ageing Cromanite™ (shown in figure 3.3) a ditched microstructure is observed, i.e., all grains are completely surrounded by ditches. This indicates severe susceptibility to intergranular corrosion attack. This result confirms the findings reported by several workers that nitrogen content in excess of 0.25 wt % significantly increases the degree of sensitisation by precipitation of chromium nitrides[46,50,85-87].

The stain-free austenitic microstructure of AISI 304 in a solution treated condition (shown in figure 3.2) indicates a carbide-free structure. This is classified as a step structure which indicates immunity to intergranular corrosion attack. The dual structure of the AISI 304 aged condition (shown in figure 3.4) represents an

inconclusive result as far as immunity to intergranular corrosion attack is concerned.

The microstructure of AISI 304 (see figure 3.5) in the solution annealed condition revealed the presence of a small amount of delta-ferrite while that of Cromanite™ in the same condition (shown in figure 3.6) showed no retained ferrite when etched in 20% NaOH. This confirms the ability of nitrogen to fully stabilise the austenite phase in the absence of nickel.

Reduction in the amount of interstitial solid solution elements, carbon and nitrogen minimises susceptibility to sensitisation while increasing the tendency toward delta-ferrite stabilisation[88]. This is the case with the AISI 304 SS used in this work, which has ten times less (C+ N) than Cromanite™. Other studies have also found that small amounts of delta-ferrite in austenitic stainless steels improve their resistance to intergranular corrosion attack because $M_{23}C_6$ precipitates at austenite-ferrite phase boundaries rather than at the austenitic grain boundaries and the former are not prone to preferential attack[89].

5.2 General corrosion

The corrosion resistance of a material depends on its chemical composition, microstructure and the environment to which it is exposed. When two materials are compared, they must have been exposed to the same heat treatment condition. The significance of this is that, for a given chemical composition and surrounding environment, there is an optimum corrosion resistance for the microstructure

5.2.1 Materials in 1N H_2SO_4.

Figure 4.1 shows the potentiodynamic scans of the solution treated Cromanite™ and AISI 304 stainless steel samples in 1N sulphuric acid. The materials show closely comparable corrosion behaviour. The passive region, which determines the potential range at which the material passivates, is very similar for both samples. The passive current density trend which indicates the stability of the film, is indistinguishable between the two samples.

The critical current density of Cromanite™ is higher than that of AISI 304 stainless steel by ten orders of magnitude. This result has been found by other workers and they have attributed it to the inability of nitrogen to counteract the increase in critical current density as a result of manganese additions[1,39-40].

AISI 430 is included for comparison to illustrate the difference in corrosion behaviour of austenitic and ferritic stainless steels. Both Cromanite™ and AISI 304, which are austenitic SS, show lower passive current density than AISI 430. This indicates that Cromanite™ has a more stable passive film in this solution than AISI 430 ferritic SS.

Figure 4.2 shows the potentiodynamic scans of the aged Cromanite™ and aged AISI 304 SS also tested in 1N H_2SO_4. The stainless property, i.e. passive region, is retained for both materials. However, passive current density and critical current density differ significantly when compared to those of the solution treated samples. This suggests that both materials suffered from degradation of corrosion properties on being aged.

This degradation results from the formation of precipitates (chromium carbides and/or carbo-nitrides) along the grain boundaries during ageing. These precipitates are rich in chromium, which has diffused from the areas immediately adjacent to the grain boundaries. These areas become depleted in Cr leading to a Cr differential between the grain boundary and the interior of the grain. During the forward polarisation the grain boundary area is less protected hence it becomes anodic and corrodes preferentially. This results in faster overall corrosion rates of the aged samples as observed in table 4.1.

This result is consistent with the observation found on etching aged samples in according to ASTM A 262-91[75] Practice A standard test (seen in figures 3.3 and 3.4). The corrosion scans (see figure 4.2) do not however, differentiate between the aged samples, as would be expected from the difference in appearance of these optical micrographs. In addition the difference in corrosion rates of aged materials is very small when the scatter in measuring corrosion rates is considered. This failure of corrosion rates to differentiate between these samples which evidently have different degrees of sensitisation is due to the fact that corrosion currents are measured at open corrosion potential, E_{corr}, whereas to measure sensitisation passive or transpassive behaviour must be considered[90].

5.2.2 Materials in salt solution

Figure 4.3 shows potentiodynamic scans of solution treated Cromanite™ and AISI 304 SS samples in 3 M NaCl solution. The materials show a similar passive range. Cromanite™ shows slightly higher pitting potential than AISI 304 though it is apparent that the corrosion potential, E_{corr} of Cromanite™ is shifted towards a more active direction in comparison with that of AISI 304 SS. The passive film of Cromanite™ will be expected to be slightly more stable than that of AISI 304 SS

since the passive current density for Cromanite™ is lower than that for AISI 304 SS.

Figure 4.4 shows potentiodynamic scans for both the solution treated and aged experimental alloys in an acidified salt solution (0.05 M HCl + 3 M NaCl). The aged specimens showed only active corrosion state for both alloys. This is due to the aggression of the solution used which could not permit any comparison on these aged samples. The critical current densities for both aged samples are very large. Although figure 3.4 showed very little precipitation of carbides in the aged AISI 304 SS when compared to aged Cromanite™ (figure 3.3), its corrosion resistance in 0.05 M HCl + 3 M NaCl solution was severely reduced. The corrosion rates presented in table 4.2 show a similar general trend to those in table 4.1 though the scatter in measurements remains high.

Figure 2.15 (p. 26) showed that nitrogen has no direct influence on the general corrosion properties of stainless steel[3] though there still appears to be a fair amount of controversy on the subject[44]. The results found in this study suggest that the consequence of replacing nickel with nitrogen is a loss in the general corrosion properties of the alloy. This is reflected by the consistently low corrosion rates found for type AISI 304 stainless steel. The same figure 2.15 shows that nickel is involved in reducing both maximum current density and passive current density together with increasing the pitting potential.

Stanko et al[32] also showed that nickel is effective in reducing the corrosion rates in stainless steels, as illustrated in figure 2.11 (p. 20). Fourie[33] suggested a nominal amount of 2 wt % Ni in order to avoid the high corrosion rates associated with the absence of nickel. However, it is worth noting that the passive behaviour for both Cromanite™ and AISI 304 stainless steels was found to be the same.

5.2.3 Sensitisation measurements

Whether sensitisation is computed by measuring the total charge Q normalised to grain boundary area, Pa, or the ratio of the peak currents during anodic scan and reactivation scan, R_a(%), the underlying principle used is the same. This principle involves measuring the total charge or current needed to break and reform the passive layer. These methods are based on the behaviour of a material in the passive or transpassive regions and not at the open–circuit corrosion potential[90].

5.2.3.1 Solution treated specimens

The Pa values of both Cromanite™ and AISI 304 are classified as unsensitised microstructures according to table 4.4. This is to be expected because of the absence of precipitates at the grain boundaries in the solution treated samples. EPR method is suitable for comparison only when there is a Cr-depleted zone of less than 13 wt % Cr and larger than 200 angstrom[54].

Figures 3.1 and 3.2 present the microstructures of Cromanite™ and AISI 304 SS samples respectively, both in the solution treated condition. The two microstructures show no preferential attack at the grain boundaries for both samples which indicates immunity to intergranular corrosion attack.

Typical R_a(%) values found by some other workers for AISI 304 stainless steel varied from 0.0% for unsensitised samples to 25.0% for severely sensitised samples[54,80]. The R_a(%) values of the solution treated samples for both materials confirms the immunity to intergranular corrosion attack.

5.2.3.2 Aged Samples

According to ASTM G108-92[83], aged AISI 304 SS has a Pa value which indicates a slightly sensitised microstructure with limited intergranular attack and this result confirms the oxalic etch test, ASTM A 262-91[75] Practice A, which is shown in figure 3.4. The double-loop method, which gives the R_a(%) value, also confirms the above results. Other workers have reported similar values for the same ageing time[79]. However the microstructure (figure 4.7) shows a moderately to heavily sensitised microstructure rather than the slight sensitisation suggested by the classification scheme based on the Pa value (Table 4.4).

This is not viewed as a contradiction since the classification scheme of Pa values has been suggested only as a general guide. Moreover ASTM A262-91[75] Practice A is not a quantitative test. It is sufficient to conclude from this test that aged AISI 304 SS is susceptible to intergranular corrosion. The microstructure evaluation after the EPR test is regarded as a better criterion than the classification scheme.

The microstructure of the aged Cromanite™, shown in figure 4.6, confirms that the high Pa value is caused by severe pitting and grain boundary attack. The R_a(%) value obtained for the aged Cromanite™ is higher than those obtained in related studies where nitrogen was added in nickel-bearing stainless steels[80]. However the maximum nitrogen content for these studies was only 0.25 wt % while for the high nitrogen Cr-Mn SS, Cromanite™, under investigation the nitrogen content is twice this amount.

Several studies using the EPR test have found that nitrogen additions of up to 0.16 wt % retard sensitisation of austenitic stainless steels, whereas nitrogen additions from 0.16 to 0.25 wt % progressively promote sensitisation[85]. This present investigation confirms that nitrogen additions in excess of 0.16 wt % are no longer beneficial but contribute to the extent of localised chromium depletion.

A recent study[90] on high nitrogen Cr-Mn SS showed similarly high Pa values, which compare very well with those found in this present study at a similar heat treatment condition. It was also reported that ageing high-nitrogen Cr-Mn SS at 800°C for times greater than 30 hours resulted in sensitisation values that decreased continuously with further ageing up to 300 hours. This reduction in sensitisation with increased ageing time after peak DOS has been reached is called healing. This is a well known phenomena in carbon alloyed AISI 304 SS, where it is associated with $M_{23}C_6$ formation. The healing process therefore also applies to high-nitrogen Cr-Mn SS in which case it is associated with Cr_2N precipitation.

Clearly, control of sensitisation is the single most important aspect which needs attention in the development of high nitrogen stainless steels if they are to compete with nickel bearing stainless steels, such as AISI 304 stainless steel. A substantial amount of work on decreasing the amount of carbon and nitrogen available for formation of chromium carbides and nitrides has been reported[91-93]. This is achieved mainly by the introduction of elements that form carbides or nitrides, such as Ti, Nb and V. This however will not work in the case of Cromanite™ where nitrogen in solid-solution is essential for the desired properties, e.g. workhardening rate behaviour, high strength and toughness.

5.3 Stress corrosion cracking

5.3.1 Slow strain rate test

5.3.1.1 Distilled water

The tests in distilled water showed that both materials are fully ductile. The maximum elongation for these materials does not differ significantly. The superiority of Cromanite™ in both strength and work-hardening rate is demonstrated by figures 4.8 and 4.9. The fracture surfaces of both these materials show that these materials are immune to any form of degradation of mechanical properties in this environment. Hence the selection of this condition as an inert environment is a valid one.

5.3.1.2 Salt solution (3M NaCl)

AISI 304 SS in 3M NaCl solution showed very little degradation in mechanical properties as characterised by little deviation of UTS_N and EL_N (Table 4.6) from unity. RA_N which is a very sensitive parameter for SCC susceptibility also indicates immunity of this material in this environment. The fractography shown in figure 4.11 confirmed the absence of stress corrosion cracks.

On the other hand Cromanite™ showed stress corrosion cracking in this solution, as observed in the micrograph shown in figure 4.12a. Payer et al.[72] suggested that the presence of secondary cracks which are perpendicular to the applied stress are a clear indication of SCC. This secondary cracking together with these perpendicular cracks (figure 4.12d) were observed in this material. The degradation of ductility as shown in Table 4.5 by the EL_N parameter in particular, is further evidence. The RA_N parameter, also shown in Table 4.4 indicated marked deviation from unity which confirmed susceptibility of this material in this solution.

It is widely accepted that SCC involves three stages : an induction period, an initiation period of microcracks, and crack propagation. The slow strain rate

method is known to eliminate the induction period and as a result considered to be too aggressive to be correlated to real plant conditions. Nucleation of cracks is especially important for stainless steels because of the existence of passive film. The nucleation and propagation of cracks should therefore be connected with formation and rupture of the surface film. The next question appears to be directed at the nature of the surface film in Cromanite™ which allowed SCC cracking, as opposed to the nature of the film developed in AISI 304 SS.

This can be addressed by analysing the composition of the surface film in these materials or by studying the repassivation behaviour of these films. Ahila et al.[44] found the surface film developed on high-nitrogen Cr-Mn to be enriched in nitrogen which they believed may lead to desorption of aggressive Cl^- anions. This is supported by their findings which showed these steels to have a better repassivation behaviour than Cr-Ni SS. However, substantial amounts of work done on Cr-Mn surface films suggest the opposite[39-40,42]. Devasenapathi et al.[39] reported that Cr-Mn SS with equal Cr content do not exhibit the same passivation as Cr-Ni SS. These authors found that the reduction of nickel is directly related to the SCC susceptibility and as the amount of Ni approaches 4 wt % SCC resistance approaches that of AISI 304 SS. Stanko et al.[32] also found that when Ni content approaches 4 wt % corrosion rates of Cr-Mn SS becomes similar to those of conventional AISI 304 SS. These results which are very consistent with each other, seem to predict the findings in the present investigation.

Figure 2.14 (p. 25) shows the findings of Pedrazzoli and Speidel[46] regarding the effect of nitrogen and carbon on stress corrosion cracking of austenitic SS. These findings suggested that nitrogen additions to SS do not affect SCC but

carbon increases the SCC susceptibility[50]. This can only be true if both nitrogen and carbon are in solid solution, i.e., there is no sensitisation. It is also known that pure metals are immune to SCC[88] and that any addition of elements in solid

solution makes these metals susceptible to SCC. Therefore the reduction of carbon content in Cromanite™, which is still very high in carbon should benefit the SCC resistance of the alloy.

5.3.1.3 0.05M HCl + 3M NaCl solution

Cromanite™ suffered even more from stress corrosion cracking in this solution. Cracking covered the entire fracture surface area of the specimen (see figure 4.14). Mechanical properties were greatly degraded, as indicated by the EL_N parameter in particular (see Table 4.5). The RA_N parameter showed marked deviation from unity which indicated that the material became more susceptible as the concentration of aggressive species increased.

AISI 304 SS started suffering from stress corrosion cracking in this solution. The fracture surface micrograph (see figure 4.13a) showed a characteristic branching nature. This is confirmed by the presence of secondary cracks along the gauge length of the specimen. A transverse section of this specimen showed that these secondary cracks are perpendicular to the applied stress. The RA_N parameter (Table 4.6) showed a significant deviation from unity which indicates susceptibility to SCC. The EL_N also showed marked deviation from unity, which indicates the degradation of mechanical properties in this solution.

Zang et al.[2] found that AISI 304 SS is susceptible to stress corrosion cracking in acid chloride (Cl^-) solutions. They found that a film enriched in Cr and Ni protected the base of the metal. Nucleation of cracks was found to be connected with the formation and build-up of a high local concentration of Cl^- ions.

According to Ahila et al.[44], Cr-Mn SS should behave better under these conditions because of the enrichment of nitrogen in the films, which leads to

desorption of the aggressive Cl^- anions upon breakdown of the passive film. This enrichment has been found by several workers[39,40,50,53].

SCC is believed to occur when the strain rate just balances the rate of repassivation[39,72-73]; otherwise SS undergo general corrosion due to lower repassivation or show SCC resistance due to higher repassivation rates. Clearly it is the repassivation rate of the film which is important rather than the composition. The ability of a metal to repassivate after the passive film breakdown determines its resistance to localised failures. This therefore suggests that scratching techniques are very suitable method to measure repassivation. It is also possible to eliminate errors due to hydrogen or oxygen evolution encountered in the case of other electrochemical techniques[40], if the scratching technique is employed.

5.3.1.40.15M / 0.5 HCl + 3M NaCl

The higher corrosion rates dominated the failure of Cromanite™ (see figures 4.15 and 4.17) in solutions containing HCl at concentrations of 0.15 M and above. Table 4.4 shows that there was a significant mass loss in Cromanite™ in these solutions. This made it impossible for SCC to be assessed.

AISI 304 SS showed very little mass loss though it suffered stress corrosion cracking in these solutions. The notable feature is that the extent of susceptibility increased slightly when compared with Cromanite™. The aspect of stress vs. strain curves (figures 4.8 and 4.9) demonstrate this very well.

5.3.2 Bent - beam test

Static tests were performed for both the solution treated and aged samples, in a 0.05 M HCl + 3 M NaCl solution. The polarisation curves are shown in figure 4.4. While the solution treated samples showed passive behaviour in this solution their aged counterparts showed active corrosion states.

The tensile stresses necessary for SCC are static. This makes the bent-beam method a realistic method to simulate the conditions in an engineering application that cause SCC. In this study two materials were compared for relative susceptibility. The conditions chosen must be severe enough to produce varying degrees of cracking in the alloys.

The bent-beam test is least used to study SCC for the following reasons : firstly, the crevicing of the specimen in the holder[84]; secondly, the possibility of inconclusive results if the tests are terminated after some cut-off time without specimen failure[58]; thirdly the possibility of the specimen relaxing during the test, thus producing a complicated stress profile which makes the analysis of stress difficult. The first problem was dealt with in this work by epoxy coating the holder. The second problem was overcome by making the test solution very aggressive. The specimens were monitored for relaxation and tightened accordingly at weekly intervals.

The bent beam test was carried out in a 0.05 M HCl + 3 M NaCl solution. AISI 304 SS and Cromanite™ in the solution treated condition were both immune to stress corrosion cracking in this solution after 100 days as shown in figure 4.19. However the degree of corrosion degradation differed slightly between the two materials.

The anodic curves for both these solution treated materials in this solution (figure 4.4) showed limited passive region. The microstructures (figure 4.19) reveal general corrosion as the mode of failure rather than stress corrosion cracking.

This indicates that Cromanite™ in the solution treated condition is not susceptible to cracking after 100 days. It is worth noting however that SSRT showed cracking in both AISI 304 and Cromanite™ in this same solution (see figures 4.14 and 4.15). This is not entirely surprising. Daniels[71] compared the results found on using SSRT, constant displacement test and constant load test on the same specimens in the same environment and the author found that the three techniques gave different results. The author suggested that in order to predict SCC performance with confidence, one must use more than one technique. Yang et al.[66] also demonstrated variations when they found that susceptibility to SCC decreased with increasing temperature in the range 200 to 300°C when assessed with the constant displacement test, but susceptibility increased up to a maximum at 250°C when assessed by SSRT. They proposed that the oxide formed on the SS in high temperature water is enhanced in nickel content for SSRT but no significant nickel enhancement occurs in the oxides formed on constant displacement test[67].

Tests on aged samples were investigated in the same solution. Cracking was observed in Cromanite™ after only 25 days as seen in figure 4.20. One specimen in three had cracked at the end of this period and the cracks were still shallow though they had passed the initiation stage. After 50 days all tests on Cromanite™ were discontinued because all 3 specimens had failed as shown in figure 4.21.

AISI 304 in the aged condition had not cracked after 75 days of exposure; however the corrosion damage was severe (see figure 4.22). The main difference between the aged specimens is the degree of sensitisation, as discussed in section 5.2.3.2. It is now well established that when high-nitrogen Cr-Mn SS are heated at temperatures between 550°C and 850°C precipitation of carbo-nitrides is promoted[46,48,-54].

Chapter 6 CONCLUSIONS AND RECOMMENDATIONS

This project is a preliminary investigation of corrosion and stress corrosion properties of this high-nitrogen Cr-Mn SS, Cromanite™. The experimental design took this into consideration. The purpose of any stress corrosion testing is to simulate on a small scale the conditions, i.e., materials, stress and environment, that exist in an engineering application. This can either be for evaluation of a particular alloy for a specific application or to compare the relative behaviour of several materials, as was the case in this study. This comparison was achieved by making the environment severe enough to produce varying degrees of susceptibility so that a comparative index could be obtained.

In the slow strain rate method an alternative approach would have been the use of a less aggressive solution with stringent control to determine SCC dependence on strain rate and potential. This would have been ideal, once the corrosion properties of Cromanite™ and AISI 304 SS had been established to be the same. Similarly in the bent-beam method a less aggressive solution could have been used and stress dependence of stress corrosion cracking determined.

6.1 List of conclusions

The conclusions may be summarised as follows :

1. Nitrogen in Cromanite™ fully stabilises the austenitic phase without retaining any ferrite while a small amount of ferrite is present in AISI 304 SS. This emphasises the strong austenitic stabilising effect of nitrogen when compared to nickel.

2. Solution treated samples of both Cromanite™ and AISI 304 SS are immune to intergranular corrosion according to the ASTM A 262-91 standard test.

3. After ageing at 675°C for 1hour (water quench) both stainless steel samples show a degree of susceptibility to intergranular corrosion, with Cromanite™ exhibiting severe susceptibility compared to AISI 304 SS, according to the ASTM A 262-91 standard test.

4. The potentiodynamic scans of Cromanite™ and AISI 304 stainless steel in the solution treated condition and their aged counterparts indicate comparable passivity properties in all environments tested.

5. Corrosion rates from Tafel plots showed Cromanite™ in both heat treatments to have significantly higher corrosion rates than AISI 304 SS, even though the scatter associated with corrosion rate calculations was high.

6. The EPR test revealed no sensitisation for both Cromanite™ and AISI 304 SS in the solution treated condition. This is consistent with the results from the ASTM A 262-91 standard test.

7. Cromanite™ is highly susceptible to sensitisation. Heat treating at 675°C for 1 hour (water-quench) led to a high degree of sensitisation. This was indicated by a high Pa value of 0.46 Ccm^{-2} from the single-loop method and a high R_a(%) value of 36.68% from the double-loop method. The microstructural evaluation from a single-loop method confirmed that these high DOS values resulted from major grain boundary pitting in the aged Cromanite™.

8. On ageing, AISI 304 SS exhibits a moderate degree of sensitisation which was indicated by a value of 0.21 Ccm^{-2} from the single-loop method and a R_a(%) value of 16.41 % from the double-loop method. This is consistent with the moderate grain boundary attack observed in the ASTM A 262-91 standard test.

9. The EPR method is a sensitive method in detecting sensitisation after heat treatment. Both variations of the EPR method were found to be well suited for the task at hand.

10. When assessed with SSR technique Cromanite™ cracked in 3 M NaCl solution while AISI 304 only started cracking when 0.05 M HCl was present in the 3 M NaCl solution.

11. Although SSRT produced cracking for both materials in solution treated samples in 0.05 M HCl + 3 M NaCl solution, the bent-beam test did not show any cracking under these conditions. SSRT is therefore too aggressive a tool for the meaningful evaluation of SCC. It is, however, a very useful means of determining relative SCC susceptibility in shorter times.

12. Fractography and metallography provide the single most important parameter to evaluate cracking in the SSRT method. All the aspects of stress-strain curves are secondary and only useful to determine the degree of susceptibility once cracks have been observed.

13. The bent-beam test showed that both samples in the solution treated condition were immune to stress corrosion cracking even after 100 days in the 0.05 M HCl + 3 M NaCl solution. Cromanite™ in the aged condition cracked after only 25 days in this environment while aged AISI 304 SS did not crack after 75 days.

14. The bent-beam test is the more realistic method to determine SCC because it utilises static stresses (not dynamic stresses such as in SSRT) which are similar in nature to those in engineering applications.

6.2 List of recommendations

On the basis of the results of this investigation and the literature review, the following recommendations are made:

1. Nitrogen benefits to SCC corrosion cracking are that the addition of nitrogen allows low carbon SS to be produced[46]. Carbon content in the alloy under investigation can be reduced to exceptionally low levels to exploit the benefits of nitrogen addition.

2. The unique synergistic effect of addition of molybdenum and nitrogen should be exploited in increasing the corrosion resistance of the alloy. The amount of 1 wt % Mo has been found to be sufficient to improve the passivation behaviour of the high nitrogen Cr-Mn alloy[1] when compared to AISI 304 SS.

3. Introduction of nickel seems inevitable at this current stage of research on stress corrosion properties of high-nitrogen Cr-Mn SS. Nickel has been found to have a positive influence both on corrosion rates[33] and stress corrosion properties[39] of the Cr-Mn SS. A minimum of 2 wt % is necessary for optimal resistance to stress corrosion and corrosion in general. This nickel amount is possible without decreasing the nitrogen solubility in the SS melt.

4. There is an overwhelming evidence that nitrogen in excess of 0.24 wt % decreases SCC resistance[40,45,53,85,90] while an increase from this amount is beneficial to strength, toughness and wear behaviour[15-17] of a high-nitrogen Cr-Mn stainless steel. This suggests that a decrease in nitrogen content which will not compromise strength, toughness and wear should be investigated for possible benefit to SCC.

References

1. Premachandra, K., De Klerk, H. J., Levey, P.R. and De Villiers, W. M., SAIMM, 1996, pp. 570-576.

2. Fang, Z., Wu, R., Cao, B. and Xiao, F., Corrosion, Vol. 50, No. 11, 1994, pp. 873-878.

3. Sedricks, A. J. (1979) Corrosion of stainless steels. John Wiley and Sons.

4. Castro, R. (1993) Historical background to stainless steels. De Physique Les Ulis. France, pp. 1-9.

5. Andrews, R., Journal of the Iron and Steel Institute, Vol. 184, 1956, pp. 414.

6. Truman, J. E. (1992) Constitution and Properties of Stainless Steels, VCH, Germany, pp.538

7. Peckering, D. and Bernstein, I. (1977) Handbook of Stainless Steels, McGraw-Hill Inc., USA, pp.1.6.

8. Simmons, J.W., Atteridge, D.G. and Rawers, J.C., Corrosion Science, 1994, Vol. 50, No.7, pp. 491-501.

9. Lacombe, P. and Beranger, G. (1993) Structure and Equilibrium Diagrams of Various Stainless Steels, Stainless Steels, Les Editions de Physique, France, pp. 47-58.

10. Espy, R.H., Welding Journal, 1982, pp. 149.

11. Pickering, F.B. Physical Metallurgy and the Design of Steels, Applied Science Publishers Ltd., England, 1978, pp. 227-229.

12. Forch, K., Stein, G. and Menzel J., Technologies of Newly Developed High Nitrogen Steels, Proc. Into. Conf. High Nitrogen Steels, The Institute of Metals, Lillie, 1988, pp. 258-267.

13. Rawers, J.C. and Kikuchi M., Journal of Materials Engineering and Performance, Vol. 2 No. 5, 1993, pp. 51-657.

14. Irvine, K.J., Llewellyn, D.T. and Pickering, F.B. Iron Steel Inst. Vol. 199, 1961, pp.153.

15. Medovar, B.I., Sayenko, V., Medovar, L.B. and Us, V.I Proc. Into. Conf., High Nitrogen Steels, Institute of Metals, 1988,. Lillie, pp. 284-287

16. Uggowitzer, P. J., Magdowski, R. and Spiedel, M. O., Proceedings of Innovation Stainless Steel, Florence, Italy, Oct. 1993.

17. Spiedel, M.O., Proc. Into. Conf. High Nitrogen Steels, The Institute of Metals, Lillie, 1988, pp. 39-48

18. Fontana, M.G. and Greene, N.D., Corrosion Enginnering, Second Edition, McGraw-Hill, Singapore, 1978.

19. Meletis, E.J., Hochman, R.F., Corrosion Science, Vol.26, No.1, 1986, pp 63-70.

20. Brown, B.F.,Stress Corrosion Cracking of Metals-A state of the Art, ASTM STP 518, 1972, pp.3-15.

21. Newman, R.C. and Procter, R.M.P., Corrosion Journal, Vol. 25, No.4, pp. 259-263.

22. Srivatsan, T.S., Sudarshan, T.S., Journal of Material Science, Vol. 23, 1988, pp.1521-1533.

23. Rimbert, J.F., Corrosion Science, Vol. 20, No.2, 1980, pp. 189-209.

24. Sedricks, A.J. Corrosion, Vol.42, No.7, 1986, pp.377-389.

25. Ford, F.P., Burstein, G.T. and Hoar, T.P., Journal of Electrochemical Society, Vol. 127, No.6, 1980, pp.1325-1331.

26. Briant, C.L, Metallurgical aspects of environmental failures. Elsevier. Oxford. 1985.

27. Hoar, T. P.and. Hines, J.G., Journal of Iron Institute, Vol. 182, No. 2, 1956, pp. 124-143.

28. Hisamatsu, Y., Passivity and its breakdown on iron and iron base alloys, Editors Staehle, R.W., Okada, H., NACE, 1975, pp. 99-105.

29. Vaccaro, F.P., Hehemann, R.F. and Troano, A.R., Corrosion, Vol. 36, No. 10, 1980, pp. 530-537.

30. Zakroczymski, T., Fan, C.J. and Szklarska-Smialowska, Z. Journal of the Electrochemical Society, Vol. 132, No. 12, 1985, pp. 2862-2867.

31. Chen, W. and Stephens, J., Corrosion Science Vol. 35, No. 2,1993, pp. 443-449.

32. Stanko, J.S. and Wellbeloved, J., Manganese in corrosion resistant steels, Samancor, Johannesburg, 1991.

33. Fourie, J.W., Corrosion evaluation of experimental manganese containing steels, (MST(93)MC1770), CSIR, 1993.

34. Lula, R.A., ASM International, June 1993, pp. 1-12.

35. Speidel, M.O. and Uggowitzer, P.J, ASM International, June 1993, pp.135-142.

36. Levey, P.R. and van Bennekom, A., J. SAIMM, Vol. 95, No. 7, 1995, pp. 337-346.

37. Wanklyn, J.N., Corrosion Science, Vol. 21, 1981, pp. 211-219.

38. Truman, J.E., Coleman, M.J. and Pirt, K.R., Brit. Corrosion Journal, Vol. 12, 1977, pp. 236-241.

39. Devasenapathi, A., Prasad, R.C. and Raja, V.S., Journal of Materials Science, Vol. 31, 1996, pp. 3989-3939.

40. Devasenapathi, A., Ramakrishna, G.S. and Raja, V.S., Journal of Materials Science Letters, Vol. 14, 1995, pp. 233-239.

41. Eckenrod, J.J. and Kovach, C.W., Properties of Austenitic Stainless Steel and Their Weld Metals, ASTM STP 679, ASTM, Philadelphia, Pennsylavania, 1979.

42. Beneke, H.S. and Sandenbergh, R.F., Corrosion Science, Vol. 29, 1989, pp. 543-549.

43. Clarke, W.L. and Gordon, G.M., Corrosion, Vol. 29, 1973, pp. 1-6.

44. Ahila, S., Reynders, B. and Grabke, H.J., Corrosion Science, Vol. 38, No. 11, 1996, pp.1991-2005.

45. Agrawal, A.K. and Staehle, Corrosion, Vol. 35, 1977, pp. 418-423.

46. Pedrazzoli, R.M. and Speidel, M.O., Proc. Into. Conf. High Nitrogen Steels, The Institute of Metals, Lillie, May 1988, pp. 208-213.

47. Walker, M.S. and Rowe, L.C., Corrosion Science, Vol. 25, No. 2, 1969, pp. 47-54.

48. Pictorius, P.C. and Rautenbach, A.S.M., Mechanical Technology, Vol. 4, No. 1, 1996, pp. 5-9.

49. Streicher, M.A., Journal of Electrochemical Society, Vol. 103, 1956, pp. 375-381.

50. Dutta, R.S., De, P.K. and Gadiyar, H.S., Corrosion Science, Vol. 34, No. 1, 1993, pp. 51-60.

51. Parkins, R.N., Corrosion Science, Vol. 52, No.5, 1996, pp. 363-374.

52. Mayo, W.E., Materials Science and Engineering, A232, 1997, pp. 129-139.

53. Mozhi, T.A., Clark, W.A.T. and Wilde, B.E., Corrosion Science, Vol. 27, No. 3, 1987, pp. 257-273.

54. Mozhi, T.A., Clark, W.A.T., Nishimoto, K., Johnson, W.B. and MacDonald, D.D., Corrosion, Vol. 41, No. 10, 1985, pp. 555-561.

55. Jones, D.A., Corrosion Science, Vol. 52, No.5, 1996, pp. 356-362.

56. Anderson, P.L. and Briant, C.L., Corrosion Science, Vol. 45, No. 6, 1989, pp. 448-463.

57. Weeks, J.R., Corrosion Science, Vol. 25, No. 9, 1985, pp. 757-763.

58. Kowaka, M. Metal Corrosion Damage and Protection Technology. New York, Allerton Press, 1990.

59. Petch, N.J. and Stables, P., Nature, Vol. 169, 1952, pp. 93-100.

60. Nichols, H. And Rostoker, W., Acta Metallurgica, Vol. 9, May 1962, pp. 491-503.

61. Silcock, J.M., Corrosion, Vol. 38, No. 3, 1982, pp. 144-156.

62. Sieradzki, K. and Newman, R.C., J. Phys. Chem. Solids, Vol. 48, No. 11, 1987, pp. 1101-1113.

63. Logan, H.L., The Stress Corrosion of Metals. Wiley, New York, 1966.

64. ASTM G39-90 (1993). Standard practice for preparation and use of bent-beam stress corrosion specimens.

65. Tsurata, T. and Okamoto, S., Corrosion Vol. 48, No. 6, 1992, pp. 518-527.

66. Yang, W., Zhang, M., Zhao, G. and Congleton, J., Corrosion, Vol. 47, No. 4, 1991, pp. 226-233.

67. Yang, W., Zhao, G., Zhang, M. And Congleton, J. Corrosion Science, Vol. 33, No. 1, 1992, pp. 89-102.

68. Tokiwai, M., Kimura, H. and Kusanagi, H., Corrosion Science, Vol. 25, No.9 1985, pp. 837-844.

69. Parkins, R.N., Mazza, F., Royuela, J.J. and Scully, J.C., British Corrosion Journal, Vol. 7, 1972, pp.154-166.

70. Parkins, R.N., Development of Slow Strain-rate testing, ASTM, STP 665, 1979, pp. 5-25.

71. Daniels, W.L., Comparative findings using the slow strain rate, constant flow stress and U-bend stress corrosion techniques. ASTM, STP 665, 1979, pp. 347-361.

72. Payer, J.H., Berry, W.E. and Boyd, W.K., Evaluation of Slow Strain Rate test. The Slow-Strain Rate Technique, ASTM STP 665, pp. 61-77.

73. Beavers, J.A. and Koch, G.H., Corrosion, Vol. 48, No. 3, 1992, pp. 256-264.

74. Steward, J., Wells, D.B., Scott, P.M. and Williams, D.E., Corrosion Science, Vol. 33, No. 1, 1992, pp. 73-88.

75. ASTM A262-91 (1993). Standard practice for detecting susceptibility to intergranular attack in austenitic stainless steels.

76. ASTM G5-87 (1993). Standard reference test method for making Potentiodynamic Anodic Polarisation Measurements.

77. ASTM G61-87 (1993). Polarisation measurements for localised corrosion.

78. Stern, M. and Geary, A.L., Journal of the Electrochemical Society, Vol. 104, No. 1, 1957, pp. 56.

79. Huang, H., Liu, C. And Chen, S., Corrosion, Vol. 48, No. 6. 1992, pp. 509-513.

80. Muraleedharan, P., Gnanamoorthy, J.B. and Prasad-Rao, K. Corrosion, Vol. 45, No. 2, 1989, pp. 142-149.

81. ASTM E112-88 (1993). Standard Test Methods for Determining Average Grain Size.

82. Jargelius, R.F.A., Hertzman, S., Symniotis, E., Hanninen, H. and Aalotonen, P., Corrosion, Vol. 47, No. 6, 1991, pp. 429-435.

83. ASTM G108-92 (1993). Standard Test for Electrochemical Reactivation for detecting sensitisation of AISI Type 304 and 304L Stainless Steels.

85. Betrabet, H. S, Nishimoto, K., Wilde, B.E. and Clark, W.A.T., Corrosion, Vol. 43, No. 2, 1987, pp. 77-84.

86. Thorpe, S.J., Ramaswami, B. and Aust, K.T., Corrosion, Vol. 43, No. 1, 1987, pp. 534-538.

87. Levey, P.R. and van Bennekom, A., Corrosion, Vol. 51, No. 12, 1995, pp. 911-920.

88. Davis, J.R., Stainless steels. ASM International. 1996.

89. Sui, G., Charles, E.A. and Congleton, J., Corrosion Science, Vol. 38, No. 5, 1996, pp. 687-703.

90. Covino, Jr., B.S., Cramer, S.D., Russell, J.H. and Simmons, J.W, Corrosion, Vol. 53, No. 7, 1997, pp. 525-536.

91. Karlsson, L., Henjered, A, Andren, H.O and Norden, H., Materials Science and Technology, Vol. 1, 1985, pp. 337-340.

92. Boothby, R.M., Materials Science and Technology, Vol. 2, 1986, pp. 78-85.

93. Wen-Tai, H. and Honeycombe, R.W.K., Materials Science and Technology, Vol. 1, 1985, pp. 390-401.

Appendix A

Grain size measurements were performed in accordance with ASTM E112-88. Two types of samples were prepared, one longitudinal to the rolling direction and one transverse to the rolling direction. Saturated oxalic acid etch was used to prepare specimens. The microscopy was linked to the monitor which was fixed with a grid pattern and care taken to ensure that the horizontal lines of the grid pattern are parallel to the surface plane of the specimen. A magnification of **X**50 was deemed suitable. Eight fields of view were randomly selected and intercepts / intersections counted. The relevant correction factor (2.4415) applied. The error in measurements was computed using applicable statistics.

The grain size calculation was performed on aged (675°C for 1 hour) samples as they reveal grain size boundaries more pronounced than their solution treated counterparts.

The ASTM grain size number found for two alloys is presented below.

Alloy	ASTM Grain Size Number
Cromanite™	4.96±0.27
AISI 304	5.03±0.30

Appendix B

The anodic and reactivation polarisation scans produced during the EPR test are given in the following figures. The calculation of the $R_a(\%)$ values uses only these curves. This calculation is demonstrated in section 3.2.4.

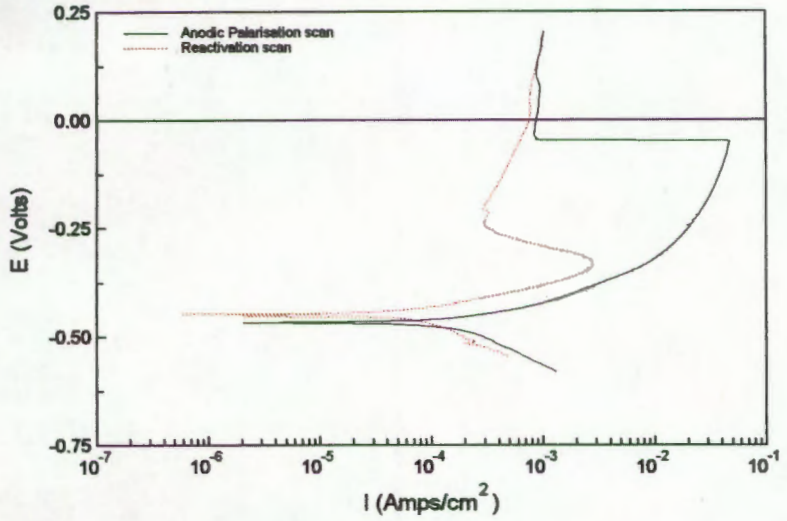

Figure 1: EPR scan for Cromanite™ in solution treated condition.

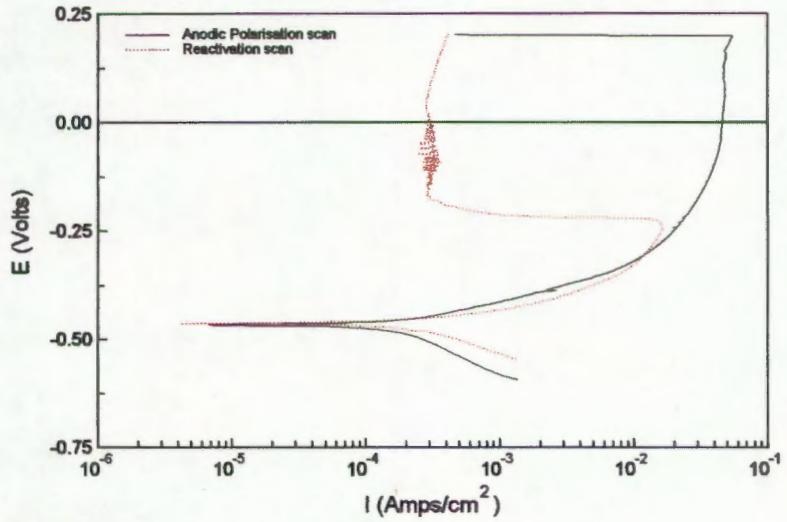

Figure 2: EPR scan for Cromanite™ sensitised at 675°C for 1 hour water quenched condition.

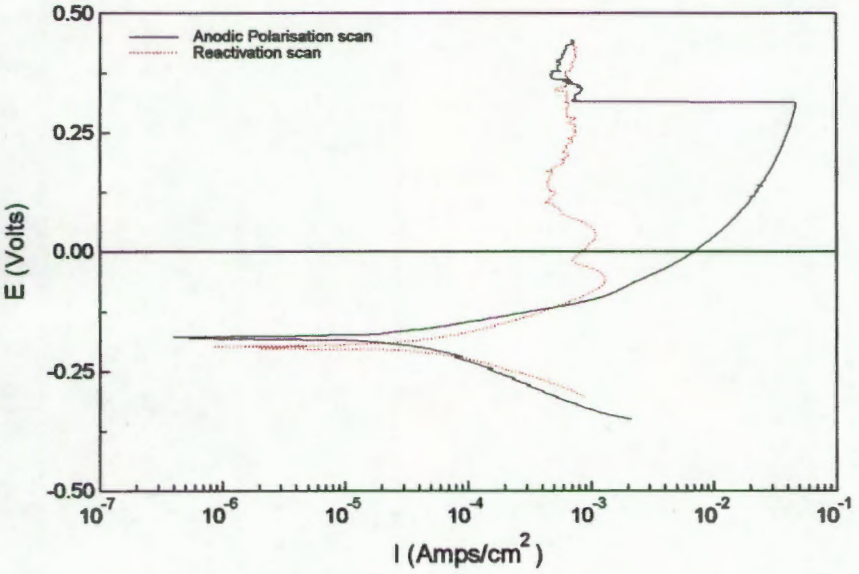

Figure 3: EPR scan for AISI 304 stainless steel in solution treated condition.

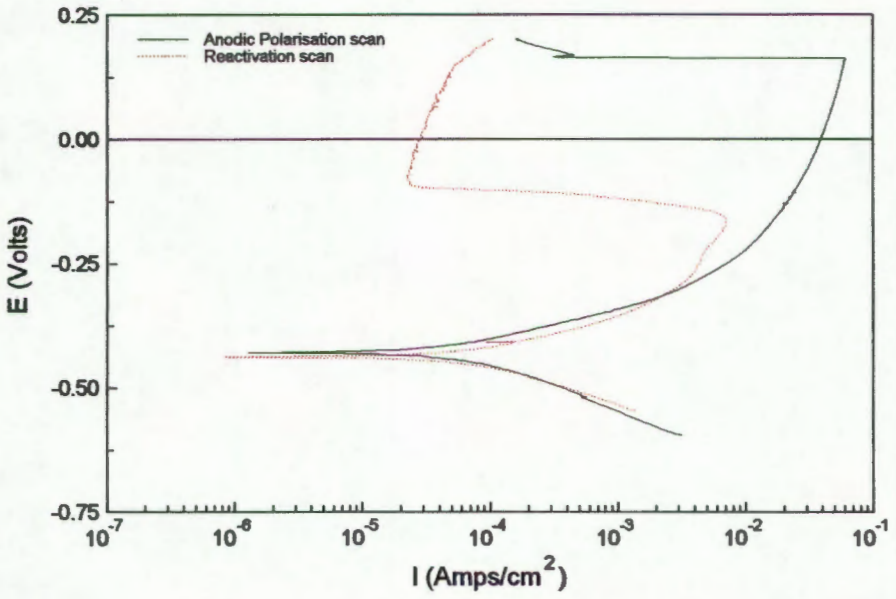

Figure 4: EPR scan for AISI 304 stainless steel sensitised at 675°C for 1 hour water quenched condition.